R. & M. No. 2930
(14,687)
A.R.C. Technical Report

MINISTRY OF SUPPLY

AERONAUTICAL RESEARCH COUNCIL
REPORTS AND MEMORANDA

High-speed Wind-tunnel Tests on Six Wings of 40-deg Sweepback, with Various Section Shapes

By

L. N. HOLMES, B.A.
and
A. B. HAINES, B.Sc.

LONDON: HER MAJESTY'S STATIONERY OFFICE
1955
PRICE 10s 6d NET

High-speed Wind-tunnel Tests on Six Wings of 40-deg Sweepback, with Various Section Shapes

By

L. N. HOLMES, B.A., and A. B. HAINES, B.Sc.

COMMUNICATED BY THE PRINCIPAL DIRECTOR OF SCIENTIFIC RESEARCH (AIR), MINISTRY OF SUPPLY

Reports and Memoranda No. 2930*

January, 1952

Summary.—Tests have been made in the Royal Aircraft Establishment High-Speed Wind Tunnel on six wings, all of the same plan form (aspect ratio 3·5, taper ratio 0·4, quarter-chord sweep 40 deg) and thickness/chord ratio (10 per cent) but of different section shapes. Four of the wings had symmetrical sections, one was cambered and one was twisted with camber varying from root to tip.

Of the symmetrical wings, the one with RAE 101 section had a much better performance than the other three (RAE 104, NACA 66A-010 and HSA I). The steep drag rise with Mach number occurred at a Mach number about 0·02 higher on the RAE 101 wing than on the next best wing (M_D for $C_L = 0·2$ was 0·91). The RAE 101 wing also had a higher lift-curve slope and more regular pitching-moment characteristics. The HSA I wing, which has a large leading-edge radius, appeared to give unsatisfactory pitching moments at a low C_L and high Mach number.

The wing with constant camber gave disappointing results, but the twisted, cambered wing had a very good performance. Compared with the symmetrical RAE 101 wing, it had higher values of M_D and lower values of drag for all values of C_L above 0·2.

It is thought that, for wings of constant section, and having the plan form and thickness/chord ratio used for these tests, the RAE 101 section is close to the optimum. However it should be possible to obtain further improvements by varying the section shape from the root to the tip.

1. *Introduction.*—The present report gives the results of tunnel tests at high subsonic speeds on six swept-back wings of the same plan form but different wing section shapes. The wings had an aspect ratio of 3·5 and a sweepback of 40 deg on the quarter-chord line. This is similar to the plan forms of several current designs. The wings had a thickness/chord ratio of 10 per cent. Five models had the same sections throughout their span; the sixth was twisted and had a camber distribution which varied throughout the span.

Many sets of two-dimensional tests have been made to compare different section shapes at high subsonic speeds, but these tests were the first three-dimensional ones to be made in this country for this purpose. Consequently in analysing the results of these tests, an attempt has been made to compare them with two-dimensional results, particularly for drag.

* R.A.E. Report Aero. 2452, received 25th March, 1952.

2. *Design of the Wings.*—The wings (Fig. 1) had a curved tip, which extended inboard for a third of the tip chord and a taper ratio of 0·4 (continuing the leading edge straight throughout the span instead of curving it).

The sections of the wings and the numbers used to denote them in this report are :

(1) RAE 101, symmetrical, maximum thickness at 31 per cent chord, theoretical minimum pressure position at $C_L = 0$, 30 per cent chord (Fig. 3).

(2) RAE 104, symmetrical, maximum thickness at 42 per cent chord, theoretical minimum pressure position at $C_L = 0$, 60 per cent chord (Figs. 2 and 3).

(3) HSA I, symmetrical, maximum thickness at 40 per cent chord. This wing was obtained by cutting off the first 1·5 per cent chord of wing No. 2 and reshaping the first 5 per cent chord of the remaining wing. This gave the wing a thickness/chord ratio of 10·15 per cent and the correct shape back to 60 per cent chord. The true HSA I section and the one tested are compared in Fig. 2. As the purpose of this test was to discover the effect of a large nose radius, this modified section was considered to be sufficiently similar to the true HSA I section.

(4) NACA 66A-010, symmetrical, maximum thickness at 45 per cent chord, theoretical minimum pressure position at $C_L = 0$, 60 per cent chord (Fig. 2). This section should be compared with RAE 104 (Fig. 2) since they were both designed to have similar pressure distributions at $C_L = 0$.

(5) RAE 101 with 1·1 per cent camber on the NACA $a = 1·0$ mean line, design $C_L = 0·2$.

(6) RAE 101 cambered on the NACA $a = 1·0$ line, and twisted about the 31 per cent chord line. Both the camber and twist distribution varied along the span, as shown in Fig. 4b. Two sections of the wing are shown in Fig. 4a. The camber was designed to neutralise the induced camber effect at a mean C_L of 0·85 at about $M = 0·80$, *i.e.*, so that the local aerodynamic centre was at the same position on the local chord at all spanwise stations. Negative twist was applied in an effort to give a spanwise lift distribution at $C_L = 0·2$ similar to that of the untwisted wings with symmetrical sections.

There were three lines of pressure-plotting holes in wing No. 6 to help in the analysis of the results. These results will be discussed more fully in a later report, but some of the overall force measurements are included in this report.

3. *Description of the Models and Tests.*—The wings were tested as half-models, using the tunnel floor as a reflection plate. The wings and body were separate, and only the forces on the wings were measured (to avoid the effects of the tunnel boundary layer). The wings passed through the tunnel floor and were fitted to a plate on the mechanical balance in the dead space. The body fitted round the stub of the wing with 0·1-in. clearance all round, and it was bolted to the turntable in the tunnel floor. A mercury seal was used to prevent air flowing through the gap between the wing and body.

Lift, drag and pitching moment were measured in all the tests. All the coefficients are based on the net wing area, since the forces measured were those on the wings only. Pitching-moment coefficients are based on the net mean chord, and are given about $0·165\bar{c}$ of the net wing*.

All the wings were tested at $R = 2 \times 10^6$ and several were tested at $R = 1 \times 10^6$ (based on the gross wing mean chord), over a Mach number range from 0·5 to 0·94. Four of the wings were sprayed with acenapthene to find the transition position by sublimation. As this method involves spraying the wing and pumping down the tunnel for each separate operating condition,

* A recent calibration of the balance has shown that all the values of C_L quoted in this report are 3 per cent too high and the values of C_m are 1·5 per cent too low.

this could only be done for a few incidences and Mach numbers. Threads were placed on wing No. 4 at 10 per cent chord to provoke forward transition, in an attempt to explain the pitching-moment behaviour of the wing. All four symmetrical wings were tested with surface tufts at a few Mach numbers.

The tests were made in October, November and December, 1949, with additional tests in November, 1950.

4. *Corrections Applied to the Results.*—The corrections applied to the observed tunnel Mach number to allow for blockage were calculated by the method given in Ref. 1. Typical values of ΔM are given in the following table.

α (deg)	M_e				
	0·50	0·80	0·85	0·90	0·94
0	0·001	0·003	0·005	0·010	0·023
6	0·001	0·004	0·007	0·014	0·030
10	0·001	0·006	0·009	0·020	—
14	0·001	0·009	0·015	—	—

Corrections were applied to lift and drag to allow for the sidewash in the tunnel.

5. *Discussion of the Drag Results.*—C_D vs. M curves at constant C_L are given in Figs. 5 and 6 and M_D vs. C_L curves in Fig. 7. M_D is defined as the Mach number at which C_D is 0·005 above the value at $M = 0{\cdot}5$ at the same C_L. To enable a better comparison of the effects of lift on drag to be made, curves of $\{C_D - (1/\pi A)C_L^2\}$ vs. C_L have been plotted (Figs. 9, 11 and 12). Since the forces on the body have not been measured, these curves cannot be used to give the ' induced drag ' factor K for the wings. However they can be used to compare the effects of different section shapes at constant C_L.

5.1. *Drag at $C_L = 0$.*—The C_D vs. M curves at $C_L = 0$ show little difference between the sections below $M = 0{\cdot}85$, but above that Mach number, wing No. 1 (RAE 101 section) is markedly better than the other wings.

For wings in two-dimensional flow, it has been found possible to correlate the values of M_D with M_{crit} at $C_L = 0$ (defining M_{crit} as the Mach number at which sonic velocity is first reached locally on the surface). In view of this, an attempt has been made to correlate the differences in M_D for the various wings used in these tests with the differences in the critical Mach numbers calculated for both the ' yawed ', *i.e.*, middle part of the semi-span and ' root ' parts of the wings.

For the yawed part of the wing, critical Mach numbers have been estimated by various rules, *e.g.*, Glauert, von Kármán and Weber using the local sweep at each chordwise position. These methods do not give the same answers but they agree quite well in estimating differences between wings. In calculating M_{crit}, two factors have to be considered :—(*a*) the value of the peak suction and (*b*) the chordwise position of the peak suction, as, because of the taper of the wings, the sweepback of a constant x/c line decreases as x/c is increased. The RAE 104 and NACA 66 sections both have their peak suctions at $x/c = 0{\cdot}6$ at $C_L = 0$, but since NACA 66 is thicker than RAE 104 aft of $x/c = 0{\cdot}45$ (Fig. 2), it has a higher peak suction. Hence NACA 66 has an M_{crit} about 0·01 lower than that of RAE 104. On the other hand, RAE 101 has an M_{crit} 0·01 higher than RAE 104, which can be analysed as a gain of 0·04 due to the forward peak suction position and a loss of 0·03 due to the higher value of the peak suction, *i.e.*, the increased sweepback due to the forward position has a greater effect than the higher value of the peak suction.

The pressure distributions which have been calculated for wings numbers 1, 2 and 4 for $M = 0{\cdot}85$ and $C_L = 0$ are shown in Fig. 8. They are presented to give an idea of the different shapes of the distributions rather than to give accurate values of C_p. These particular curves were obtained by using the von Kármán law for the yawed part of the wing.

In the root part of the wing, RAE 101 shows up to even greater advantage, for not only is its peak-suction line near the root more swept (due to the taper of the wing), but the actual value of the peak suction is lower than for the other two sections. This is because the peak suctions of RAE 104 and NACA 66 are behind the maximum thickness positions of the aerofoils, where the additional term due to the kink[2] increases the suctions, whereas for RAE 101, the peak suction position and maximum thickness position are almost coincident. The ' kink ' pressure distributions shown in Fig. 8 are those calculated for the kink of a wing without a body and would be modified by a body. The calculated M_{crit} in the root is $0{\cdot}020$ higher for RAE 101 than for RAE 104 and is $0{\cdot}015$ lower for NACA 66 than for RAE 104.

The values of M_D (Fig. 7) for these wings at $C_L = 0$ are $0{\cdot}924$ for RAE 101, $0{\cdot}904$ for RAE 104 and $0{\cdot}895$ for NACA 66. The differences between them are similar to the differences in M_{crit} calculated for the yawed parts of the wings and the root sections. Hence it appears that at $C_L = 0$, a good idea of the effects on drag due to changing the section shape of a wing can be obtained by calculating the pressure distribution and deriving values of M_{crit}. If the body and root part of the wings were modified to give the same shape of pressure distribution at $C_L = 0$ in that part of the wings as in the yawed part, the RAE 101 section wing would still be better than the RAE 104 section wing by the amount calculated for the yawed part. This is because at $C_L = 0$, the effects of taper on the local sweep are more important than the differences which would be present in two-dimensional performance.

The following table shows how the gain in M_D at $C_L = 0$ is very dependent on section shape, with the present swept wings, compared with a straight wing.

Section	M_D for $\phi = 0$ deg, $A = 5{\cdot}5$ (Ref. 4)	M_D for $\phi = 40$ deg, $A = 3{\cdot}5$	ΔM_D
RAE 101	$0{\cdot}795$	$0{\cdot}924$	$0{\cdot}13$
RAE 104	$0{\cdot}82$	$0{\cdot}904$	$0{\cdot}085$

Wing number 3 (HSA I section) has practically the same C_D and M_D at $C_L = 0$ as wing number 2 (RAE 104 section) (*see* Figs. 5 and 7). This is reasonable as these two aerofoils are similar in shape in the neighbourhood of and behind the peak suction positions.

The cambered wing (No. 5) has a slightly higher drag than the basic symmetrical wing (No. 1) (Fig. 6) at $C_L = 0$, but has the same variation with Mach number. This is a little better than would be expected from two-dimensional evidence.

For all the wings, there is a slow rise in C_D with increasing Mach number between $M = 0{\cdot}5$ and $M = 0{\cdot}85$ (Fig. 5). Tests made recently on a wing of the same plan form but $8{\cdot}5$ per cent thick, also show this slow rise, both with transition free and with transition fixed on the wing at 10 per cent chord. Hence this slow rise does not appear to be due to variations of transition position with Mach number. It is possible that at high speeds, the increase in drag at the root section is not balanced by an equal increase in thrust at the tip as in potential flow. This may be aggravated by the experimental technique of using half-models, which result in a thicker boundary layer over the body and possibly some disturbance in the wing-body junction.

5.2. *Drag at Moderate Values of Lift.*—5.2.1. *Moderate Mach numbers.*—At lift, wing number 1 (RAE 101) has appreciably less drag than the other symmetrical wings. This difference is already apparent near $C_L = 0{\cdot}2$ and becomes more marked as the lift is increased. The transition photographs (Fig. 10) for $M = 0{\cdot}5$ show that at $C_L = 0$, transition is further back on the RAE 104 wing than for the RAE 101 wing, but for $C_L = 0{\cdot}25$, transition has moved forward to near the leading edge in both cases. Hence there is a greater transition movement between $C_L = 0$ and $0{\cdot}25$ for the RAE 104 wing than for the RAE 101 wing, but this accounts for only a small part of the difference in drag between the wings at $C_L = 0{\cdot}25$.

It seems likely that as in two-dimensional tests, the main increase is due to a larger laminar separation bubble near the leading edge of the sharper nosed aerofoils at moderate lift coefficients. On a two-dimensional RAE 104 section wing at low Reynolds number, the marked increase in drag occurred at a C_L of about $0{\cdot}6$, but on a swept-back wing it would be expected to occur at a lower C_L. The NACA 66 wing has a leading-edge radius between those of RAE 101 and RAE 104 (Table 2A) and its drag over the range $C_L = 0{\cdot}2$ to $0{\cdot}4$ is also intermediate. However the leading-edge radius can be increased too far, as is shown by the results on the HSA I section. This section has a considerably larger leading-edge radius than the other sections used in these tests ($0{\cdot}014c$ in comparison with $0{\cdot}0076c$ for RAE 101), but its drag is higher than those of the other wings at lift (Fig. 5). This is probably because this section has a local peak suction near the nose even at $C_L = 0$, and with lift this peak increases rapidly, leading to a separation and increased drag. At higher Reynolds numbers, the difference in drag between all the wings at moderate values of C_L would probably be much less.

5.2.2. *High Mach numbers.*—The discussion is based on the results for $R = 2 \times 10^6$, but Fig. 14 shows that the conclusions would not be really different if the results for $R = 1 \times 10^6$ were used instead.

(*a*) *Comparison between* RAE 101 *and* RAE 104 *sections.*—The main conclusions from the C_D vs. M curves (Fig. 5) is that the steep drag rise occurs at Mach numbers $0{\cdot}02$ higher on the RAE 101 wing than on the RAE 104 wing at all values of C_L up to $0{\cdot}4$. Hence the loss in performance with increasing C_L is the same for both wings. This conclusion would not be obtained from a comparison of the values of M_D but these are not reliable at lift because of the differences in the drag at low speed. At high Mach numbers, the shape of the pressure distribution over the yawed part of the wing at lift differs from that at low speed: the high peak suctions near the leading edge (shown in the calculated 'yawed' distributions in Fig. 13) have tended to collapse and in general, there is no serious adverse pressure gradient ahead of the shock-wave which moves well back on the aerofoil. Hence the laminar separation near the leading edge of sharp-nosed aerofoils tends to disappear at high Mach numbers and so, other effects being neglected, the drag with these sections would show a reduction with Mach number. This change in shape of the pressure distribution over the yawed part of the wings is confirmed by the transition photographs (Fig. 10, $C_L \simeq 0{\cdot}25$, cf. $M = 0{\cdot}5$ and $M = 0{\cdot}88$).

However the loss on both these swept-back wings is greater than the loss two-dimensionally[4,5] and the additional loss seems to be caused mainly by the kink and tip regions, for the yawed part of the wing behaves in a similar way to two-dimensional aerofoils, as just shown. The relative importance of the root and tip regions is probably different on these two wings, as it seems that the tip region is more serious on the RAE 101 wing, but the root should be worse on the RAE 104 wing.

The pressure distributions for the root and yawed parts of the wing are compared in Fig. 13. In the root sections, the pressure distributions at lift are similar in shape to the ones at $C_L = 0$, but the suctions are higher (hence M_{crit} is lower). The increase in drag with Mach number will occur earlier on the inner parts of the wing than on the yawed part because:

(i) the isobars are less swept, and

(ii) with this rounded type of pressure distribution the drag rise usually follows soon after sonic conditions are reached on the aerofoil, whereas with the flat-topped type of distribution found in the yawed part of the wing, the drag rise is usually delayed to a higher Mach number.

The transition photographs at high Mach number (Fig. 10) are useful because it is thought that over the root and mid-parts of the wing, they give a good idea of the position of the shock-waves. For $C_L = 0{\cdot}25$, $M = 0{\cdot}88$, the transition line is much further back as a fraction of the local chord on the inner part of the wing than near the mid-semi-span, and is less swept than even the trailing edge, whereas at $C_L = 0$, $M = 0{\cdot}88$ (not given, but similar to $C_L = 0$, $M = 0{\cdot}5$) the transition line is at the same fraction of the local chord all across the wing. This shows that the adverse effects at the root have increased from $C_L = 0$.

Even at $C_L = 0$, the root was responsible for a loss in performance, particularly on the RAE 104 wing (as was seen in section 5.1) and the calculated pressure distributions in Fig. 13 show that the additional effects with increasing C_L should be more serious for RAE 104 than RAE 101. In general, the adverse effects should be worse for a section with the peak suction at zero lift aft of the maximum-thickness position, particularly if this is far back on the aerofoil. With increasing Mach number, the influence of the kink spreads progressively out along the span. Estimates show that at $M = 0{\cdot}88$, the centre effect distorts the pressure distribution shape out to about 40 per cent of the semi-span. Hence the change in shape of the pressure distribution to the more rounded root type is not merely confined to the sections very near the root, but spreads across the span with increasing Mach number, giving a reduction in effective sweep.

On the other hand, near the tips of swept wings at lift, the suctions over the forward part of the sections are higher than further inboard both because of the spanwise lift distribution and also because of distortions from the tip effect. The effects on the isobar pattern are partly alleviated by the curved leading edge but some loss of sweep may remain, particularly slightly inboard of this. Further, the higher suctions imply lower values of M_{crit}, and also the steep adverse pressure gradients behind the peak suctions may lead to a premature breakaway of flow. Comparing the two wings, the peak suctions near the tip are higher on the RAE 101 wing and there is little difference in effective sweep (confirmed to some extent by the transition photographs*). Hence the local values of M_{crit} will be lower on the RAE 101 wing and also the drag rise follows M_{crit} more closely on this wing, because the crest of the aerofoil is further forward. This relative behaviour is confirmed by the photographs of surface tufts given in Fig. 21. At $M = 0{\cdot}88$ and $C_L \simeq 0{\cdot}30$, there is a disturbed line of tufts in the probable position of the shock wave near the tip of the RAE 101 wing but there is no noticeable disturbance near the tip of the RAE 104 wing (nor, incidentally, further inboard on the 101 wing). The lift data (*see* section 6.1) also suggest that the tip effects are greater on the RAE 101 wing.

(*b*) *Performance of other sections.*—The other wings with symmetrical sections are compared most conveniently with the RAE 104 wing. For the NACA 66 wing, the variation of M_D with C_L is similar to that of the RAE 104 wing but the actual values of M_D are about $0{\cdot}01$ lower for NACA 66. Fig. 5 shows that the drag rise with Mach number is steeper. The NACA 66A-010 section has larger ordinates behind the maximum thickness and hence, particularly near the root, the peak suctions here are higher than with RAE 104 and hence M_{crit} is lower (*cf.* results for $C_L = 0$ in Fig. 8.).

The HSA I wing behaves in a similar way to the RAE 104 wing from $C_L = 0$ to $0{\cdot}2$, but above $C_L = 0{\cdot}2$, M_D decreases rapidly with increasing lift. This has also been found two-dimensionally from a comparison of the results for two sections differing in shape over the front part of the aerofoil only. These sections were 10 per cent thick, with maximum thickness at $0{\cdot}4c$, trailing-edge angle 12 deg and with leading-edge radii of $1{\cdot}1$ per cent c and $0{\cdot}7$ per cent c and so correspond to HSA I and RAE 104 respectively. In these two-dimensional tests, M_D for the section with $\varrho = 1{\cdot}1$ per cent c decreased more rapidly with increasing C_L above $C_L = 0{\cdot}3$.

* Near the tip, transition may be occurring ahead of the shock-wave—*see* the results on HSA I noted later—and so the effective sweep may be better than suggested by the transition line.

The most probable explanation is that even after a region of local supersonic flow has become established, there is still a local peak suction near the leading edge, owing to the large leading-edge radius, as well as the main peak suction ahead of the shock. This would keep transition forward (Fig. 23) and prevent the usual rearward movement with Mach number as on RAE 104 (Fig. 10), thus giving a higher drag at lift. The difference between the HSA I and RAE 104 wings at $C_L = 0{\cdot}4$ is accentuated in Fig. 7 because of the greater increase in drag on HSA I between $M = 0{\cdot}5$ and $0{\cdot}7$—this may be caused by an extension of the area of separation on this wing, referred to in section 5.2.1.

At moderate values of C_L, the cambered RAE 101 wing has a higher drag (Fig. 6) and gives lower values of M_D (Fig. 7b) than the symmetrical wing, and even at $C_L = 0{\cdot}4$ camber gives no improvement. This agrees with what has been found under two-dimensional conditions, but it had been hoped that camber might have a beneficial effect on a swept wing—even when the same amount of camber is used throughout the span. The camber should have removed the high forward peak suction at the tip which has been shown to be a main cause of the loss in M_D with lift on the symmetrical RAE 101 wing but it may have replaced this by too rounded a distribution, similar in shape to that obtained at the root (Fig. 13). The delay in the Mach number for the start of the drag rise at the tip would then be much less than the gain in $M_{c\,it}$ and may only have been sufficient to balance the rather poorer performance at the root that would be expected with a cambered section.

The twisted, cambered wing will be analysed and discussed in more detail in a later note but the significant fact is that not only did it give lower drag at high C_L (Fig. 9), but that it is as good as or better than the symmetrical, untwisted wing for C_L values as low as $0{\cdot}2$ (Figs. 6 and 7b). For $C_L = 0{\cdot}3$, for example, the steep drag rise with Mach number is delayed by about $0{\cdot}01$ in Mach number. It seems therefore that this idea is worth pursuing as this initial, somewhat arbitrary attempt improved the performance at high lift without loss to the cruising performance.

5.3. *Drag at High Values of Lift.*—At high values of C_L, all the symmetrical wings show a rapid increase in profile drag with lift above about $C_L = 0{\cdot}5$ (Fig. 9). The RAE 101 section is apparently the best in this respect, as the increase in drag occurs at a value of C_L about $0{\cdot}1$ higher than for the other sections. At high Mach number, however, the tuft photographs (and pitching-moment results) suggest that the tip stall actually starts at a lower C_L with RAE 101 and that the lower drag is due to the fact that the stall does not spread in along the wing as rapidly as with the RAE 104 section wing.

At moderate speeds and high C_L, the cambered RAE 101 wing is superior to the symmetrical RAE 101 wing, as the rapid increase in drag is delayed to a value of C_L about $0{\cdot}1$ higher. However, at high Mach numbers ($M = 0{\cdot}88$, Fig. 9 for example) the cambered wing is no better than the symmetrical wing at high values of lift, probably because the pressure distribution at the tip is too rounded, as discussed in section 5.2.2.

However the twisted cambered wing gives the best drag performance at high values of C_L at all Mach numbers (Fig. 9), and the rapid drag rise has been delayed to about $C_L = 0{\cdot}75$. This is the main evidence in favour of this type of wing.

The effects of Reynolds number on the tip stall of the symmetrical RAE 101 wing are shown in Figs. 11 and 12. At low speed ($M = 0{\cdot}18$) there is considerable Reynolds number effect between $R = 2 \times 10^6$ and $R = 6{\cdot}5 \times 10^6$ (Fig. 11a). But the results at $M = 0{\cdot}33$ and $R = 3{\cdot}5 \times 10^6$ nearly agree with those for $M = 0{\cdot}18$ and $R = 6{\cdot}5 \times 10^6$ and, allowing for Mach number effects as in Fig. 11b, there is probably little difference between curves for $R = 3{\cdot}5 \times 10^6$ and $6{\cdot}5 \times 10^6$ at $M = 0{\cdot}18$—in other words, most of the Reynolds number effects occur between $R = 2 \times 10^6$ and $R = 3{\cdot}5 \times 10^6$. At higher Mach numbers, increasing the Reynolds number from 1×10^6 to 2×10^6 delays the tip stall a little (Fig. 12). The increase in drag occurs at a C_L about $0{\cdot}06$ higher at $R = 2 \times 10^6$ than $R = 1 \times 10^6$ at $M = 0{\cdot}5$, but the effect is slightly less at higher Mach numbers.

5.4. *General Conclusions on the Section Shape to give the Best Drag Characteristics for a Wing of this Plan form.*—5.4.1. *Using the same section from the root to the tip of the wing.*—The RAE 101 section (maximum t/c at $0{\cdot}31c$, peak suction at $C_L = 0$ at $0{\cdot}30c$) is, for this plan form, the best of those tested. The steep drag rise occurs at a Mach number $0{\cdot}02$ higher with this wing than with the RAE 104 section wing. This difference is equivalent to thinning the section by $1\frac{1}{2}$ per cent in thickness/chord ratio or increasing the sweepback by about 5 deg.

The performances of wings with sections other than those tested are considered and compared with that of the RAE 101 wing below. These other sections can be divided into two groups :

(*a*) Sections with peak suctions at $C_L = 0$ and low speed ahead of that of RAE 101, *e.g.*, RAE 100 which has the peak suction at $0{\cdot}1c$ or NACA 0010, peak suction at $0{\cdot}12c$, and

(*b*) Sections with peak-suction positions between those of RAE 101 and RAE 104, *e.g.*, RAE 102, peak suction at $0{\cdot}4c$ or NACA 0010–0·70 40/1·051 peak suction at $0{\cdot}5c$.

Considering these groups in turn :

(*a*) Using a section with a far forward peak suction position at $C_L = 0$ should give a small gain in performance at $C_L = 0$ (not more than $0{\cdot}01$ in M_D) but, judging from two-dimensional data, the yawed part of the wing should be responsible for a greater loss in M_D with C_L than with RAE 101. This poorer performance should be more marked at the tips, but at the root there should be an improvement. An analysis of the available data suggests that a section of this type would be worse than RAE 101 even at moderate values of C_L, and certainly the tip stalling would be more severe at high Mach number.

(*b*) Using a section with a peak suction at $C_L = 0$ at $0{\cdot}4c$ or $0{\cdot}5c$, rather than at $0{\cdot}3c$ as with RAE 101, would result in an earlier drag rise with Mach number over the root and mid-parts of the wing. It has been estimated that the improvement near the tips would not compensate for this for values of C_L below about $0{\cdot}4$.

Therefore it seems that for operation at the cruising C_L values likely in practice ($0{\cdot}15$ to $0{\cdot}3$), little improvement over the performance of the RAE 101 wing tested is possible with any other 10 per cent thick section, if the same section is used from the root to the tip of the wing.

5.4.2. *Varying the section with position along the span.*—It should be possible to design a wing with a better performance than any of the ' constant-section ' wings discussed above, by using different sections along the span. This is a means not merely of restoring the performance at the root and tip to be as good as on the yawed part of the wing, but of increasing the effective sweep of the wing above the value of the geometric sweep of any chordwise position. In other words, the peak suction can be brought forward at the root and back at the tip more than is necessary to produce straight isobars along the wing. In the following discussion, an ' RAE 101 type wing ', etc., denotes a wing in which the modified sections are designed to give the type of pressure distribution which the RAE 101 section would have in two-dimensional flow at the same C_L, and the unmodified sections are of the RAE 101 shape. It should be noted that the actual choice of the sections depends upon the design C_L and Mach number. Appreciable gains in M_D can probably be made merely by modifying the inboard part of the wing, but to get the best performance the wing should be modified all along the span. In this case, the wing may not have any section of the basic shape.

If only the inboard part of the wing is modified, an RAE 101 type wing is preferable at low values of C_L because of its effectively greater sweep. If the design C_L were zero, it should be possible, by modifying the inboard part of the wing only, to increase M_D to $0{\cdot}94$ for an RAE 101 type wing or $0{\cdot}925$ for an RAE 104 type wing. These figures are quoted only to give an idea of the possible gain. To get an even better performance with this type of plan form, the sections should be varied throughout the span, and not merely over the inboard part. Two such wings,

have been designed and will be tested in the High-Speed Tunnel. The designs involve not only a variation in the maximum thickness position along the span, but also a variation in the thickness/chord ratio over the inboard part of the wing. Details of these wings are given in the following table to show what is needed for this type of wing.

Spanwise station (per cent semi-span)	Position of max. t/c (per cent chord)		t/c	
	I	II	I	II
12·3	15	10	0·10	0·12
20·9	35	20	0·086	0·105
30·6	38	22·5	0·090	0·102
38·9	40	27·5	0·093	0·10
50·0	42	31	0·10	0·10
88·9	50	50	0·10	0·09

It is expected that the better overall performance, particularly at low C_L, should be achieved with wing 2, which retains over mid-semi-span the RAE 101 section found above to be preferable with a 'constant-section wing'.

6. *Discussion of the Other Results.*—6.1. *Lift.*—Lift carpets for all the wings are presented in Figs. 15, 16 and 17. $(\partial C_L/\partial\alpha)_M$ is plotted against M in Fig. 18, and Reynolds number effects on the C_L vs. α curves for two Mach numbers are shown in Fig. 19. The most interesting results concerning the lift characteristics from these tests are :—(i) The RAE 101 section wings give appreciably higher values of $(\partial C_L/\partial\alpha)_M$ than the other wings, particularly above $M = 0{\cdot}85$. For example, $(\partial C_L/\partial\alpha)_M$ for the RAE 101 symmetrical wing is 6 per cent higher at $M = 0{\cdot}5$ and 26 per cent higher at $M = 0{\cdot}9$ than for the RAE 104 wing. (ii) The peak value of $(\partial C_L/\partial\alpha)_M$ occurs at a higher Mach number for the RAE 101 wings than for the other wings. This is similar to the behaviour of M_D at low C_L, as M_D was higher for the symmetrical RAE 101 wing than for the other wings.

The ratio of the lift-curve slopes at moderate speeds and low C_L for the RAE 101 and RAE 104 wings is about the same as that found on untapered, unswept wings of H.S.6 (RAE 101) and H.S.7 (RAE 104) sections and in two-dimensional tests on NACA 63 and NACA 66. Thus it seems that the difference between the lift-curve slopes is not simply a phenomenon associated with sweepback. It can probably be attributed to differences in trailing-edge angle and to the differences in the adverse pressure gradient over the forward part of the aerofoil.

The more noticeable differences between the values of $(\partial C_L/\partial\alpha)_M$ above $M = 0{\cdot}85$ are connected with the way the pressure distributions on the wings change after the appearance of shock-waves and the relative behaviour of the root and tip regions. These differences have already been discussed in relation to the drag characteristics, but are repeated briefly here where they are relevant to the behaviour of the lift.

On the RAE 101 wing, sonic velocity is first reached well forward and the flow in the local supersonic region that develops soon reaches a relatively high local Mach number and is terminated by a strong shock, even when the chordwise extent of this region is relatively small, *e.g.*, back to the maximum-thickness position. With increasing Mach number, the shock moves back, increasing the extent of the supersonic region, and this more than counterbalances the decrease in suction near the leading edge. These effects are particularly marked towards the tip, and are probably present at moderate values of C_L above $M = 0{\cdot}85$. The tuft photographs show a disturbance at the tip in the probable shock-wave position at $M = 0{\cdot}88$ and Fig. 18a shows that $(\partial C_L/\partial\alpha)_M$ for the whole wing is then still increasing with Mach number. It is likely that the local lift on the mid and tip parts of the wing increases with Mach number

until after shock-waves have appeared on the lower surface. In the same Mach number range, $(\partial C_L/\partial\alpha)_M$ has not begun to decrease on the inboard sections although an upper surface shock-wave may be present*. Hence the total effect is that the lift on this wing increases rapidly with Mach number after the flow over the tip sections becomes supersonic.

On the RAE 104 wing on the other hand, the behaviour at high Mach number is different in two important respects. First, the yawed and tip pressure distributions develop rather differently after sonic conditions are reached. The peak suction near the leading edge soon collapses, leaving a flat-topped pressure distribution with relatively low supersonic Mach numbers and the shock at about 60 per cent chord. Compared with the RAE 101 wing, the possible subsequent rearward movement of the shock is much smaller and consequently there is little further increase in lift with Mach number. Secondly, at these Mach numbers, the local lift at the root may be decreasing since the inboard part of the wing shock stalls at a relatively lower Mach number. These effects would combine to give only a small increase in the total lift of the wing after sonic conditions have been reached.

The HSA I and NACA 66 wings (numbers 3 and 4) have a variation of $(\partial C_L/\partial\alpha)_M$ with M similar to that of the RAE 104 wing. This is to be expected as, at high Mach numbers and moderate values of C_L, these wings have similar pressure distributions, particularly over the rear half of the aerofoils.

At moderate Mach numbers, the RAE 101 cambered wing behaves similarly to the symmetrical one (Fig. 18), but above $M = 0{\cdot}85$, $(\partial C_L/\partial\alpha_M)$ does not rise so much for the cambered wing, although it is still considerably higher than $(\partial C_L/\partial\alpha)_M$ for the wings of the RAE 104 group. The pressure distribution is more rounded on the cambered than on the symmetrical RAE 101 wing, consequently not as much lift is gained from the effects of the backward movement of the shock-waves there.

Reverting to moderate Mach numbers, but higher values of C_L than have been considered above, there is an increase in $(\partial C_L/\partial\alpha)_M$ with C_L for wings Nos. 1, 2 and 3 at values of C_L between $0{\cdot}4$ and $0{\cdot}6$ (*see* lift carpets Figs. 15 and 16). This characteristic has been noted before for swept wings (being more marked at angles of sweep greater than 40 deg) and is connected with a change in the flow pattern near the tips. The trailing vortices leave the wing near the leading edge instead of the trailing edge, and increase the lift over the wing. At higher values of C_L, the tip stalls and the vortex moves in from the tip, giving a decrease in $(\partial C_L/\partial\alpha)_M$ (Figs. 15 and 16). The increase in $(\partial C_L/\partial\alpha)_M$ above $C_L = 0{\cdot}4$ does not occur on the cambered wings—presumably because the suctions outboard near the leading edge are not so high on those wings—or with NACA 66A-010. With the latter, there is actually an appreciable reduction in lift curve slope above $C_L = 0{\cdot}5$. This may be caused by the effects of the steeper adverse pressure gradient with this wing on the boundary layer towards the rear of the section. The increase in $(\partial C_L/\partial\alpha)_M$ between $C_L = 0{\cdot}4$ and $0{\cdot}6$ is absent on all wings at Mach numbers above $M = 0{\cdot}85$.

The comparison in Fig. 19 of the C_L vs. α curves at $R = 2 \times 10^6$ and 1×10^6 for two Mach numbers shows that there are no marked Reynolds number effects below $C_L = 0{\cdot}4$. For the symmetrical wings, the tip stall apparently occurs at a lower C_L for the lower Reynolds number. The results of the cambered, twisted wing, which apparently indicate a better stalling performance at $R = 1 \times 10^6$ than at $R = 2 \times 10^6$, give a warning that an increase in Reynolds number may not always lead to an improvement.

6.2. *Pitching Moment.*—C_m vs. C_L curves for all the wings, at $R = 2 \times 10^6$, are given in Figs. 20, 22 and 27. Comparisons between the C_m vs. C_L curves at $R = 2 \times 10^6$ and $R = 1 \times 10^6$ are given in Fig. 28 for four wings. It should be remembered that the lift and pitching moment were measured on the net wing only, and that the coefficients are based on this,

* This has been deduced from the pressure-plotting results of the inboard section of the twisted cambered wing, which is similar to the symmetrical wing on the inboard part.

and related to the mean quarter-chord point of the net wing. Calculations show that the aerodynamic centre is about $0{\cdot}025\bar{c}$ further forward than it would have been if the forces had been measured on the gross wing and related to that.

Of the six wings tested, only one, the HSA I wing, showed any unusual behaviour in pitching moment at low values of C_L. This is discussed in detail below in section 6.2.2.

6.2.1. *Comparison between the* RAE 101, RAE 104 *and* NACA 66A-010 *wings* (*Fig.* 20).—The two principal wings of the series (RAE 101 and 104) behave similarly over the greater part of the C_L range at low speed and also at low values of C_L at high Mach numbers up to $M = 0{\cdot}92$ (up to $C_L = 0{\cdot}3$ at $M = 0{\cdot}9$ or $C_L = 0{\cdot}2$ at $M = 0{\cdot}92$). The aerodynamic centre for $0 < C_L < 0{\cdot}2$ moves back from about $0{\cdot}28\bar{c}$ at low speeds to $0{\cdot}315\bar{c}$ at $M = 0{\cdot}90$ and $0{\cdot}36\bar{c}$ at $M = 0{\cdot}92$.

At higher values of C_L, however, the C_m vs. C_L curves for the two wings diverge. As before, the differences can be interpreted by considering the way the pressure distributions develop after the appearance of shock-waves and also by considering the relative behaviour in the three parts of the wings.

On the RAE 101 wing, judging from the tuft photographs (Fig. 21), shock-waves appear at the tip before they appear on the yawed part of the wing. At moderate values of C_L near $M = 0{\cdot}90$ the shock-wave over these regions is still fairly well forward, and increasing incidence causes a backward movement in the position of the shock-wave. This makes the RAE 101 wing more stable. However with a further increase in incidence, the flow at the tip ultimately breaks down, and lift is lost there, resulting in the nose-up moment which limits the usable C_L (at $R = 2 \times 10^6$), to about $0{\cdot}6$ at high Mach number. It is interesting to notice that at $R = 1{\cdot} \times 10^6$ (Fig. 28), this nose-up moment soon changes into a more nose-down moment. It has been seen from the lift and drag data that the stalling of the tip region is really more severe at $R = 1 \times 10^6$, and presumably the stall spreads rapidly inboard. At $R = 2 \times 10^6$, on the other hand, the serious breakdown in lift is confined mainly to the tip, giving a more serious effect on C_m. This shows that care is needed in interpreting these pitching-moment curves at high values of C_L. At low speed, the lift and pitching-moment curves were practically unaltered by increasing the Reynolds number from 2×10^6 to 6×10^6.

On the RAE 104 wing, however, the tufts on the yawed part of the wing become disturbed before those at the tip (Fig. 21) and it is likely that the characteristics of the yawed part (essentially two dimensional characteristics) are mainly responsible for the loss in stability which occurs at moderate values of C_L at high Mach number, for example, above about $C_L = 0{\cdot}3$ at $M = 0{\cdot}90$. In the discussion on the drag data, it was explained that under these conditions, the shape of the pressure distribution on the yawed part of this wing is flat-topped with a moderate shock (and transition) back at about $0{\cdot}6c$. This was true at $C_L = 0{\cdot}25$, $M = 0{\cdot}88$ (Fig. 10) and probably applies to values of C_L below that at which the change in stability occurs. As the incidence is increased, the shock tends to occur further forward (comparing the pressure distributions on RAE 104 two-dimensionally[3]). A nose-up change in pitching moment would result. The tuft photographs for $M = 0{\cdot}92$, for example, show that above $C_L = 0{\cdot}3$, the boundary layer towards the rear of the section becomes seriously disturbed, presumably behind the strong shock. At still high incidences, this shock may be further back or the separation behind may become more serious and as a result, the pitching-moment curve turns nose-down (Fig. 20). With these effects on the yawed part and also a worse performance at the root, it is not surprising that no tip-stalling effects are apparent in the C_m vs. C_L curves. Qualitatively, there are no serious differences between the C_m data for this wing at $R = 2 \times 10^6$ and $R = 1 \times 10^6$ (Fig. 28)—this conclusion would be expected from the above description.

The C_m vs. C_L curves for NACA 66A-010 are much more irregular than those for RAE 104 at all Mach numbers above $0{\cdot}80$. In general, it seems that the effects noted for RAE 104

occur on NACA 66 at lower values of C_L or M (*e.g.*, contrast $M = 0{\cdot}9$, $C_L = 0{\cdot}5$, RAE 104 and $M = 0{\cdot}9$, $C_L = 0{\cdot}25$, NACA 66 (Fig. 20)—it was found that the behaviour of surface tufts was similar in these two cases). The loss in stability, probably due to the effects of a forward movement of the upper-surface shock with incidence, now occurs in the low C_L range. For example, for $M = 0{\cdot}92$, the aerodynamic centre (net wing) for $C_L = 0{\cdot}2$ is at $0{\cdot}275\bar{c}$ compared with $0{\cdot}36\bar{c}$ for RAE 104 or 101. By $M = 0{\cdot}94$, there is a serious nose-up change over a small range of C_L near $C_L = 0$. It is thought that this is caused by the relative movement of the upper and lower-surface shock-waves with incidence and is the characteristic which has been observed frequently on unswept wings. Remembering the pressure distribution shapes estimated for a lower Mach number at $C_L = 0$ (Fig. 10), it is likely that this effect is most pronounced near the root of the wing. The same characteristic is present at $M = 0{\cdot}94$ with the RAE 104 section but to a lesser extent—however, at $C_L = 0$, this wing is 8 per cent less stable than the RAE 101 wing. A further increase in Mach number might accentuate the effect on RAE 104.

It is clear from the above discussion that, except for the greater tip-stalling tendency, the RAE 101 wing gives the best pitching-moment characteristics. Hence a section with a far forward peak suction at $C_L = 0$ is favoured, provided the same section is used from root to tip. Reliable predictions cannot be made of the pitching-moment characteristics of the new wings that have been designed (section 5.4) with sections varying from root to tip. The modifications at the root should be sufficient to postpone the serious loss in stability near $C_L = 0$ to beyond $M = 0{\cdot}94$, but the reduction in stability at moderately high values of C_L found with the present wings may still be evident, particularly with wing 1.

6.2.2. *Comparison between* RAE 104 *and* HSA I *wings* (*Figs.* 22-25).—The pitching-moment curves for wings numbers 2 and 3 (RAE 104 and HSA I sections) are compared in Fig. 22. At moderate Mach numbers, there is little difference between the results for the two wings, but at high Mach numbers, there is a marked kink in the HSA I curves at about $C_L = 0{\cdot}2$. To investigate the reasons for this, transition pictures were taken at $M = 0{\cdot}92$ at three incidences corresponding to $C_L = 0{\cdot}14$, $0{\cdot}20$ and $0{\cdot}27$ and marked as A, B and C in Fig. 22. The photographs are shown in Fig. 23. There is no appreciable change in transition position on the lower surface, but on the upper surface there is a marked variation with increasing C_L. At A, transition takes place at about 70 per cent chord, but at B the transition has moved forward to about 15 per cent chord over most of the wing except near the tip, and at C it is slightly further forward and the effect has spread into the tip region. Before the acenapthene had fully evaporated in the turbulent layer, a thin black line appeared at about 70 per cent chord in both B and C. This effect had almost disappeared by the time the photographs shown in Fig. 23 were taken. The acenapthene, however, did not evaporate as quickly behind this line as in front of it and some of the residue can be seen in Fig. 23—particularly in B. It is thought that this line indicates the position of the shock-wave and there is a slower rate of evaporation behind it either because of the thicker boundary layer or the presence of a separation behind the shock. Therefore the forward movement of transition is not associated with a forward movement of the main shock-wave. Since on the smooth surface of these model wings transition must be an indication of an adverse pressure gradient, this suggests that even at this Mach number (0·92), there is still a local peak suction near the leading edge from about $C_L = 0{\cdot}2$ on this section with the large leading-edge radius.

After seeing these photographs, a transition thread was put on the wing at 10 per cent chord, first on the upper surface only and then on both surfaces. The results at $M = 0{\cdot}92$ are shown in Figs. 24 and 25. For C_L values above the kink in the C_m vs. C_L curve, transition free, all three results are in reasonable agreement as would be expected since the natural transition position (Fig. 23) is well forward. Fixing transition on the upper surface only makes the C_m vs. C_L curve straighter but there is a large positive $C_{m\,0}$ and a positive shift of about 0·6 deg

in the no-lift angle. These effects at zero lift are caused by a modification of the pressure distribution shape due to fixing transition (*see* below) and not merely due to having made the wing asymmetrical. Putting a thread on both surfaces restores $C_{m\,0}$ and the no-lift angle to about their original values, as the pressure distributions are similar on both surfaces again near $C_L = 0$ and the C_0 vs. C_L curve is now smooth between $C_L = 0$ and $0{\cdot}25$. There is however a considerable change of stability with C_L—the aerodynamic centre varies from $0{\cdot}245\bar{c}$ at $C_L = 0$ to $0{\cdot}39\bar{c}$ at $C_L = 0{\cdot}3$.

The reason for the kink in the C_m vs. C_L curve, transition free (and for the large $C_{m\,0}$, etc., when transition is fixed forward on the upper surface only), seems to be connected with the type of boundary-layer flow ahead of the main shock. With transition far back, as in A, there is laminar flow back to near the shock-wave, and there is a gradual pressure recovery, possibly through a multi-shock system. When transition is far forward, as in B, there is a turbulent layer ahead of the shock and consequently there is probably a strong single shock.

The results with transition fixed on both surfaces may be the closest to those obtained in flight, although the method of fixing transition may give an unrealistically thick boundary layer. It is likely that the pitching-moment characteristics on a swept wing with HSA I sections may be unsatisfactory in practice at high Mach number. It is true that the section tested was not the true HSA I section aft of $0{\cdot}6c$ (Fig. 2), but these pitching-moment effects are due to conditions near the leading edge of the section, and so are likely to be found with the true HSA I section.

No tests were made with transition fixed on the RAE 101 or RAE 104 wings. However, it is not expected that fixing transition would have much effect on the pitching-moment data at low and moderate values of C_L, on these wings. In support of this, no appreciable differences have been obtained in recent tests with transition free and fixed on a wing of this plan form but with $8{\cdot}5$ per cent thick RAE 101 sections.

6.2.3. *The effects of camber and twist.*—The C_m vs. C_L curves for the symmetrical, cambered and cambered-twisted wings with RAE 101 sections are compared in Fig. 27 and the variation of $C_{m\,0}$ with Mach number is given in Fig. 26.

The wing with a uniform amount of camber throughout the span, and no twist, has characteristics very similar to those of the symmetrical wing, except for its value of $C_{m\,0}$ which varies from $-0{\cdot}032$ at $M = 0{\cdot}5$ to $-0{\cdot}057$ at $M = 0{\cdot}94$. The pitching-moment curves do not show the improvement at high lift and moderate Mach numbers, which would have been expected, judging from the drag curves (section 5.3 and Fig. 9).

The twisted, cambered wing is also disappointing. Despite the large reduction in drag at high values of C_L, the maximum usable lift is still limited to about $C_L = 0{\cdot}6$, as beyond this value there is a nose-up moment change. This will be discussed in more detail in the later note on this wing.

Fig. 28 shows that reducing the Reynolds number from 2×10^6 to 1×10^6 has a large effect on the C_m–C_L data at high Mach number for these wings. The differences at high values of C_L are much larger than for the symmetrical wings, and so it is possible that the comparisons at $R = 2 \times 10^6$ give a misleading idea of the usefulness of the twisted, cambered wing in improving the pitching-moment characteristics.

It is interesting to notice that $C_{m\,0}$ for the twisted, cambered wing is almost independent of Mach number in the range tested (Fig. 26). Redesign of the wing with less positive camber at the tip and some negative camber at the root would reduce the value of $C_{m\,0}$ (about $-0{\cdot}04$ in the present design). It seems that this type of wing can be used without having large changes in $C_{m\,0}$ with Mach number.

7. *Conclusions.*—7.1. Of the four wings with symmetrical sections, the one with RAE 101 section gives the best characteristics in general (Figs. 5 and 20). Its advantages are :—

(*a*) The steep drag rise occurs at Mach numbers 0·02 higher than on the best of the other wings.

(*b*) This wing gives lower values of drag at lift than the other wings, at all Mach numbers.

(*c*) The C_m vs. C_L curves are reasonably linear up to $C_L = 0{\cdot}6$ at all Mach numbers within the range of the tests. The main disadvantage of this wing is its more serious tip-stall. This limits the usable C_L to about 0·6, but this may be less serious at higher Reynolds numbers.

(*d*) $(\partial C_L/\partial\alpha)_m$ is higher for this wing, particularly above $M = 0{\cdot}85$, and the peak of the $(\partial C_L/\partial\alpha)_m$ vs. M curve occurs at a Mach number 0·02 higher than for the other wings.

7.2. The RAE 104 section wing is superior to the NACA 66 section wing (*e.g.*, the steep drag rise occurs at Mach numbers about 0·01 higher), principally because it is thinner aft of the maximum-thickness position.

7.3. The HSA I section wing is the most unsatisfactory of the four symmetrical section wings tested. The large leading-edge radius leads to a loss in stability at low and moderate values of C_L at high Mach number, even when transition effects have been eliminated.

7.4. At $C_L = 0$, it has been found possible to correlate the effects of section shape on the Mach number at which the drag rises steeply with the values of M_{crit} calculated for the yawed and root parts of the wings. The calculations showed that for a given aspect ratio and quarter chord sweep, the choice of section is closely linked with the taper ratio. The better performance of the RAE 101 section wing (*see* section 7.1 (*a*)) near $C_L = 0$, is mainly due to the higher effective sweep of the peak-suction line (a consequence of the taper).

The loss in performance at the root, particularly at lift, is more serious for sections with peak suctions at $C_L = 0$ aft of the maximum thickness, for these sections lead to a loss in sweep of the isobars on the inner part of the wing. Hence the RAE 104 wing is worse than the RAE 101 wing in the root, and the NACA 66 wing is worse than the RAE 104 wing.

7.5. As a result of these tests and calculations, it is concluded that if the same section is to be used throughout the span on a wing of the present plan form, RAE 101 section will give about the best performance. However, it should be possible to make considerable gains by changing the section throughout the span, having in the root, a section with its maximum thickness far forward, and at the tip, a section with its maximum thickness far back.

7.6. With a cambered section throughout the span there was a reduction in M_D at moderate values of C_L, and no improvement at high values of C_L and high Mach numbers.

7.7. The twisted cambered wing gave a large improvement in drag at high values of C_L, and was at least as good as the symmetrical RAE 101 wing down to $C_L = 0{\cdot}2$, but there was no improvement in the maximum usable C_L, determined by the C_L at which the nose-up instability occurs. However there was no variation in $C_{m\,0}$ with Mach number.

REFERENCES

No.	*Author*	*Title, etc.*
1	J. Y. G. Evans	Corrections to velocity for wall constraint in any 10 × 7-ft rectangular subsonic tunnel. R. & M. 2662. April, 1949.
2	D. Kuchemann	Wing junction, fuselage and nacelles for sweptback wings. R.A.E. Report Aero. 2219. A.R.C. 11,035. August, 1947.
3	E. W. E. Rogers, C. J. Berry and R. F. Cash.	Tests at high subsonic speeds on a 10 per cent thick pressure-plotting aerofoil of RAE 104 section. Part II : Pressure distributions and flow photographs. R. & M. 2863. February, 1951.
4	E. W. E. Rogers, C. J. Berry and R. F. Cash.	Tests at high subsonic speeds on a 10 per cent thick pressure-plotting aerofoil of RAE 104 section. Part I : Force coefficients. R. & M. 2863. April, 1951.
5	R. Hills and F. N. Kirk	A summary of some recent two-dimensional aerofoil tests at high subsonic *M*. R.A.E. Tech. Note Aero. 1987. A.R.C. 12,259. February, 1949. (Unpublished.)

TABLE 1

Leading Dimensions

Half Wing

Gross area of wing (*i.e.*, from centre-line chord to tip chord)	3·94 sq ft
Net area of wing (*i.e.*, from root chord to tip chord)	3·355 sq ft
Centre-line chord	25·68 in.
Root chord	24·02 in.
Tip chord (theoretical)	10·32 in.
Gross mean chord	18 in.
Net mean chord	17·17 in.
Span	31·5 in.
Aspect ratio	3·5
Taper ratio	0·4
Sweepback of quarter-chord line	40 deg
Thickness/chord ratio	0·10
Distance of net mean quarter-chord point aft of leading-edge centre-line	19·45 in.
Distance of pitching-moment axis aft of leading-edge centre-line	18 in.

Wing Sections

(1)	RAE 101	(Model No. 101/2)
(2)	RAE 104	(,, ,, 101/3)
(3)	HSA I	(,, ,, 101/7)
(4)	NACA 66A-010	(,, ,, 101/5)
(5)	RAE 101 cambered	(,, ,, 101/4)
(6)	RAE 101 twisted and cambered	(,, ,, 101/6)

Body

Length	70·0 in.
Radius of circular middle section	3·4 in.

TABLE 2A

Section Ordinates of Wings 1 to 5

Wing No.	1	2	3	4	5	
x/c	*y/c*	*y/c*	*y/c*	*y/c*	*yu/c*	*yl/c*
0·0125	0·0137	0·0121	0·0163	0·0114	0·0148	0·0126
0·025	0·0192	0·0170	0·0210	0·0152	0·0210	0·0173
0·05	0·0266	0·0236	0·0271	0·0209	0·0298	0·0234
0·10	0·0361	0·0323	0·0343	0·0292	0·0412	0·0309
0·15	0·0422	0·0383	0·0399	0·0353	0·0489	0·0355
0·20	0·0463	0·0426	0·0440	0·0400	0·0541	0·0385
0·25	0·04885	0·0457	0·0470	0·0436	0·0578	0·0399
0·30	0·0500	0·0479	0·0491	0·0464	0·0597	0·0402
0·35	0·0495	0·0493	0·0503	0·0483	0·0598	0·0392
0·40	0·0480	0·0499	0·0508	0·0495	0·0587	0·0373
0·45	0·0457	0·0499	0·0506	0·0500	0·0566	0·0345
0·50	0·0427	0·0490	0·0498	0·0497	0·0537	0·0316
0·55	0·0392	0·0472	0·0479	0·0487	0·0501	0·0282
0·60	0·0353	0·0447	0·0449	0·0467	0·0460	0·0246
0·65	0·03115	0·0404	0·0404	0·0430	0·0415	0·0208
0·70	0·0268	0·0353	0·0353	0·0379	0·0365	0·0171
0·75	0·0224	0·0297	0·0297	0·0318	0·0312	0·0136
0·80	0·0179	0·0238	0·0238	0·0253	0·0254	0·0104
0·85	0·0134	0·0179	0·0179	0·0190	0·0194	0·0074
0·90	0·0089	0·0119	0·0119	0·01265	0·0132	0·0046
0·95	0·0045	0·0060	0·0060	0·0063	0·0068	0·0022
1·00	0	0	0	0	0	0
L.E. radius	0·0076	0·0059	0·0140	0·0066	0·0076	
T.E. Angle	10·22°	13·58°		14·5°		
Section	RAE 101	RAE 104	HSA I tested	NACA 66A-010	RAE 101 cambered according to NACA $a = 1·0$ mean line	

y = semi-ordinate of symmetrical section, yl = lower surface ordinate,

yu = upper surface ordinate.

TABLE 2B

Section Ordinates of Wing 6

	$\eta = 0{\cdot}2$		$\eta = 0{\cdot}5$	
x/c	yu/c	yl/c	yu/c	yl/c
0	0	0	0	0
0·125	0·0140	0·0134	0·0151	0·0123
0·025	0·0198	0·0186	0·0216	0·0168
0·05	0·0277	0·0255	0·0307	0·0225
0·10	0·0378	0·0344	0·0427	0·0295
0·15	0·0444	0·0400	0·0509	0·0335
0·20	0·0490	0·0436	0·0565	0·0361
0·25	0·0518	0·0458	0·0603	0·0373
0·30	0·0533	0·0467	0·0625	0·0375
0·35	0·0529	0·0461	0·0628	0·0362
0·40	0·0516	0·0444	0·0618	0·0342
0·45	0·0494	0·0420	0·0598	0·0316
0·50	0·0464	0·0390	0·0569	0·0285
0·55	0·0429	0·0355	0·0533	0·0251
0·60	0·0389	0·0317	0·0491	0·0215
0·65	0·0345	0·0277	0·0444	0·0188
0·70	0·0301	0·0235	0·0393	0·0143
0·75	0·0254	0·0194	0·0339	0·0109
0·80	0·0206	0·0152	0·0281	0·0077
0·85	0·0156	0·0112	0·0221	0·0047
0·90	0·0106	0·0072	0·0155	0·0023
0·95	0·0056	0·0034	0·0086	0·0004
1·00	0	0	0	0

$$\eta = \frac{\text{distance from centre-line}}{\text{semi-span}}$$

TABLE 2B—*continued*

Section Ordinates of Wing 6

	$\eta = 0{\cdot}8$		$\eta = 0{\cdot}89$	
x/c	yu/c	yl/c	yu/c	yl/c
0	0	0	0	0
0·0125	0·0166	0·0108	0·0171	0·0103
0·025	0·0242	0·0142	0·0251	0·0133
0·05	0·0352	0·0180	0·0366	0·0166
0·10	0·0502	0·0220	0·0524	0·0198
0·15	0·0603	0·0239	0·0634	0·0210
0·20	0·0679	0·0247	0·0714	0·0212
0·25	0·0731	0·0245	0·0770	0·0206
0·30	0·0764	0·0236	0·0807	0·0193
0·35	0·0775	0·0215	0·0820	0·0170
0·40	0·0771	0·0189	0·0818	0·0142
0·45	0·0755	0·0159	0·0802	0·0112
0·50	0·0727	0·0127	0·0775	0·0079
0·55	0·0690	0·0094	0·0737	0·0047
0·60	0·0644	0·0062	0·0691	0·0015
0·65	0·0591	0·0031	0·0636	−0·0014
0·70	0·0532	0·0004	0·0575	−0·0039
0·75	0·0467	−0·0019	0·0506	−0·0058
0·80	0·0395	−0·0037	0·0430	−0·0072
0·85	0·0317	−0·0048	0·0346	−0·0078
0·90	0·0230	−0·0052	0·0252	−0·0074
0·95	0·0131	−0·0041	0·0145	−0·0055
1·00	0	0	0	0

$$\eta = \frac{\text{distance from centre-line}}{\text{semi-span}}$$

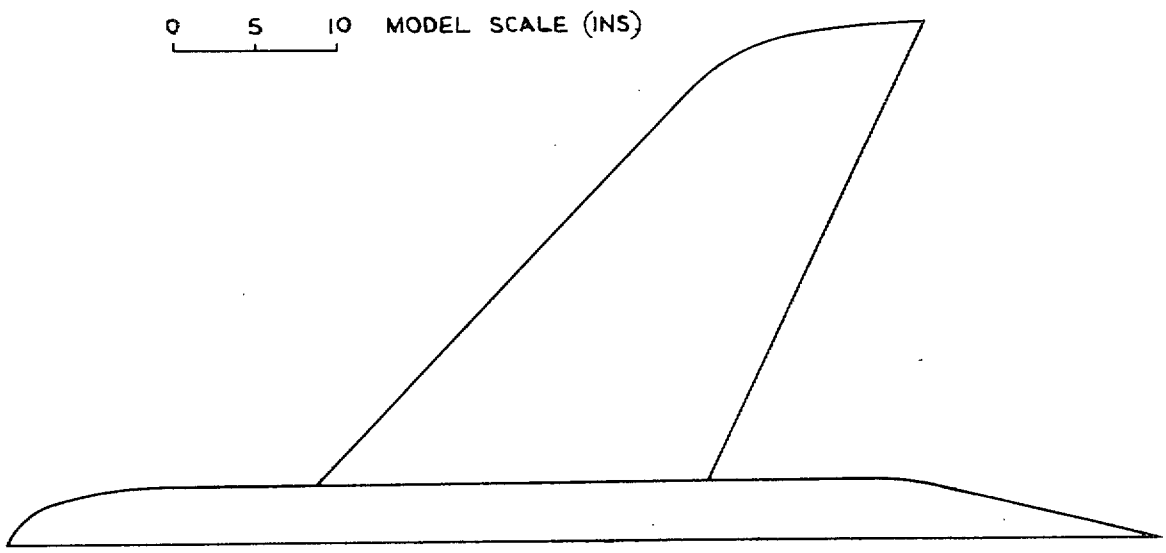

FIG. 1. The wing and body in plan view.

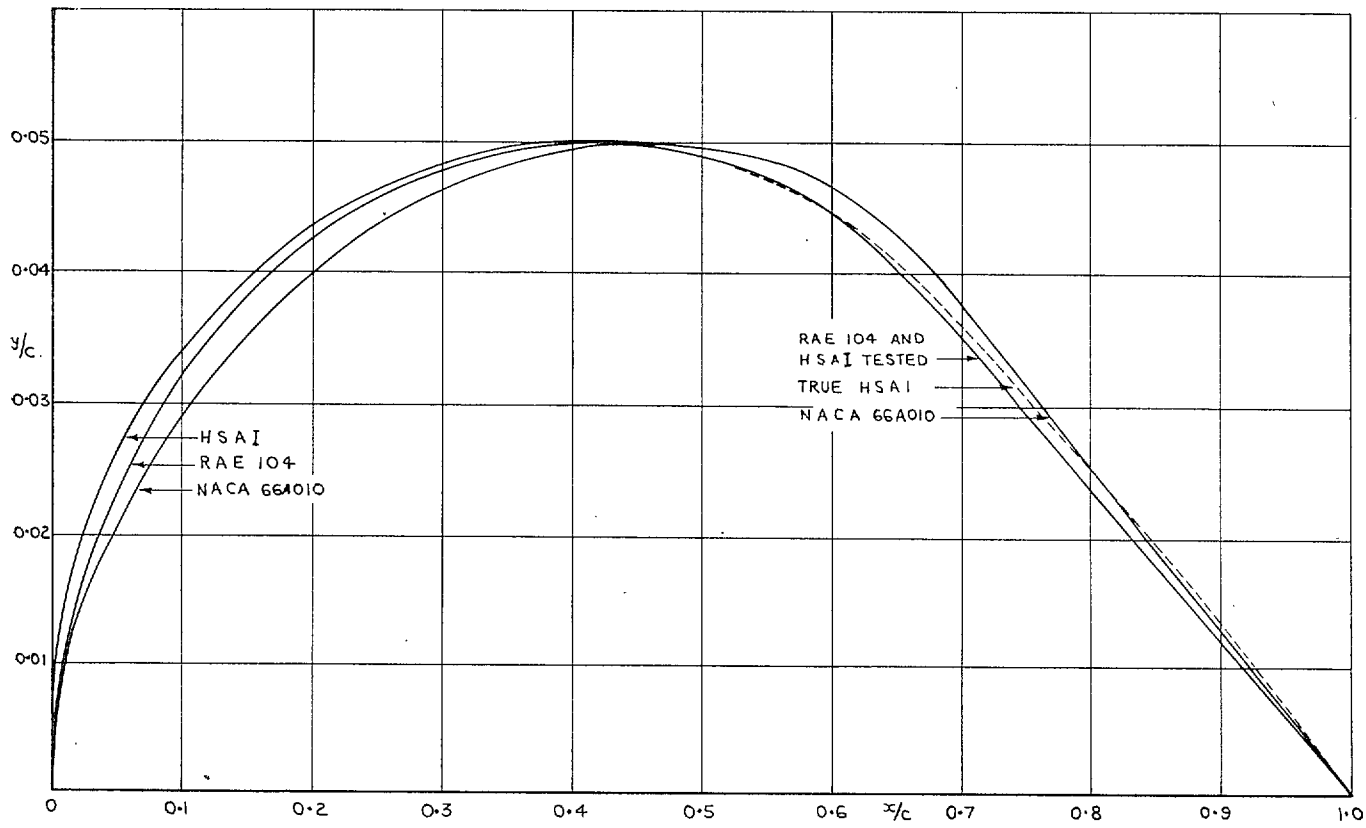

FIG. 2. A comparison between RAE 104, HSA I and NACA 66A-010 sections.

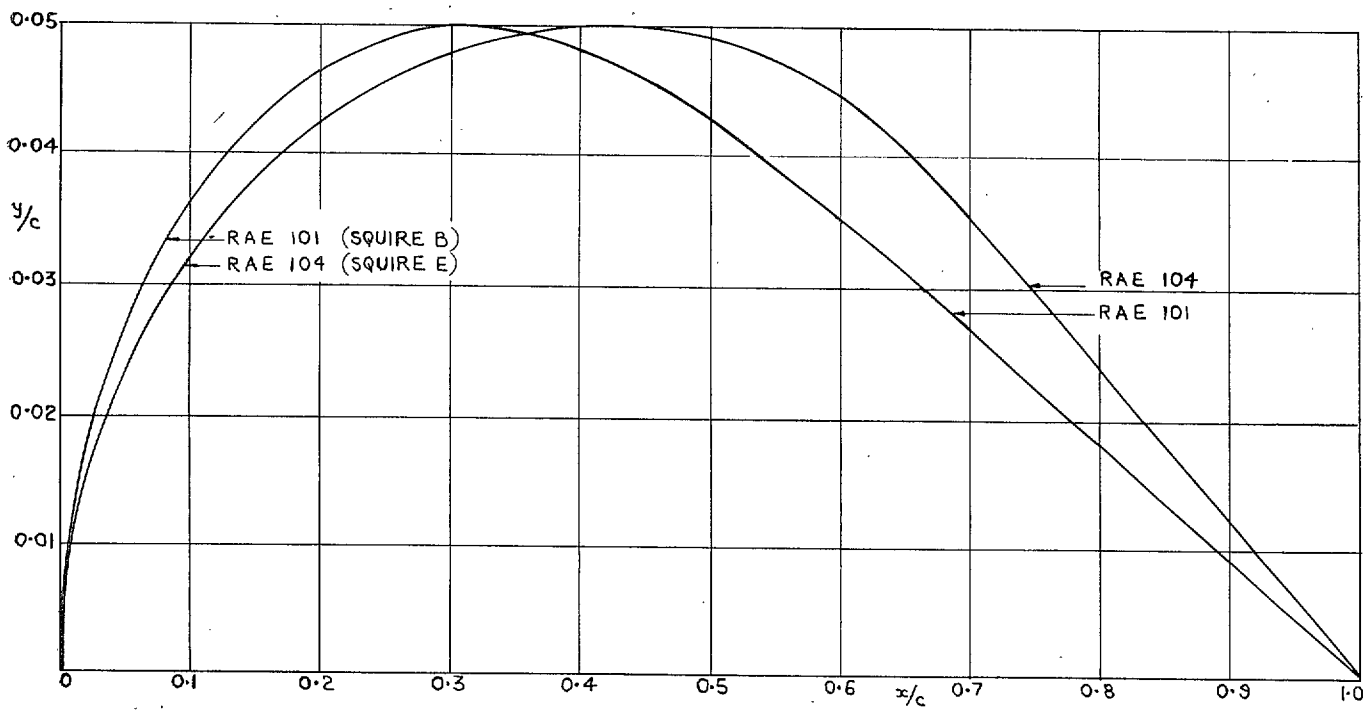

FIG. 3. A comparison between RAE 101 and RAE 104 sections.

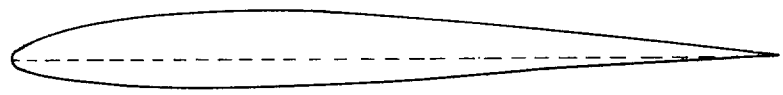

SPANWISE POSITION $\eta = 0.5$

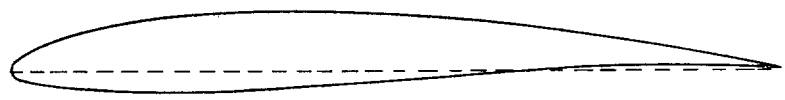

$\eta = 0.8$

FIG. 4a. Two sections of the wing.

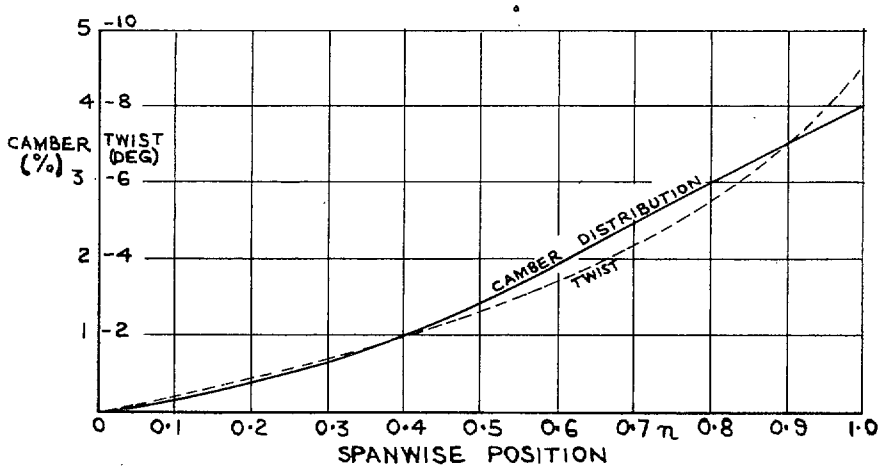

FIG. 4b. Camber and twist distribution on the wing.

FIGS. 4a and 4b. Details of wing No. 6.

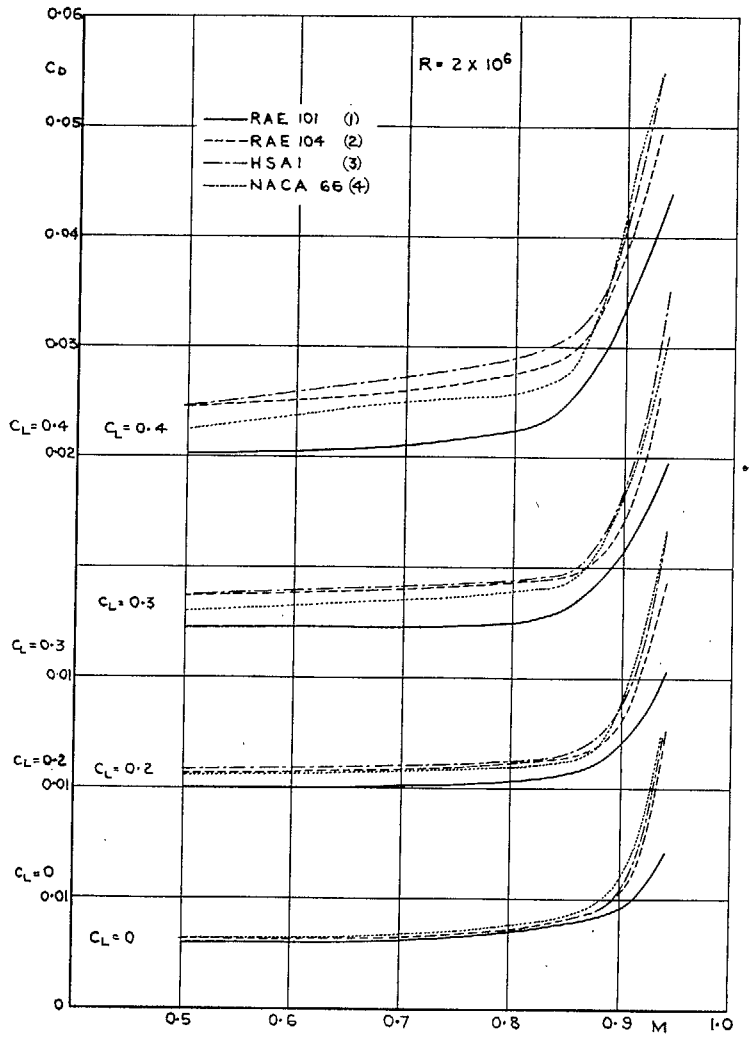

FIG. 5. C_D vs. M at constant C_L for the symmetrical wings.

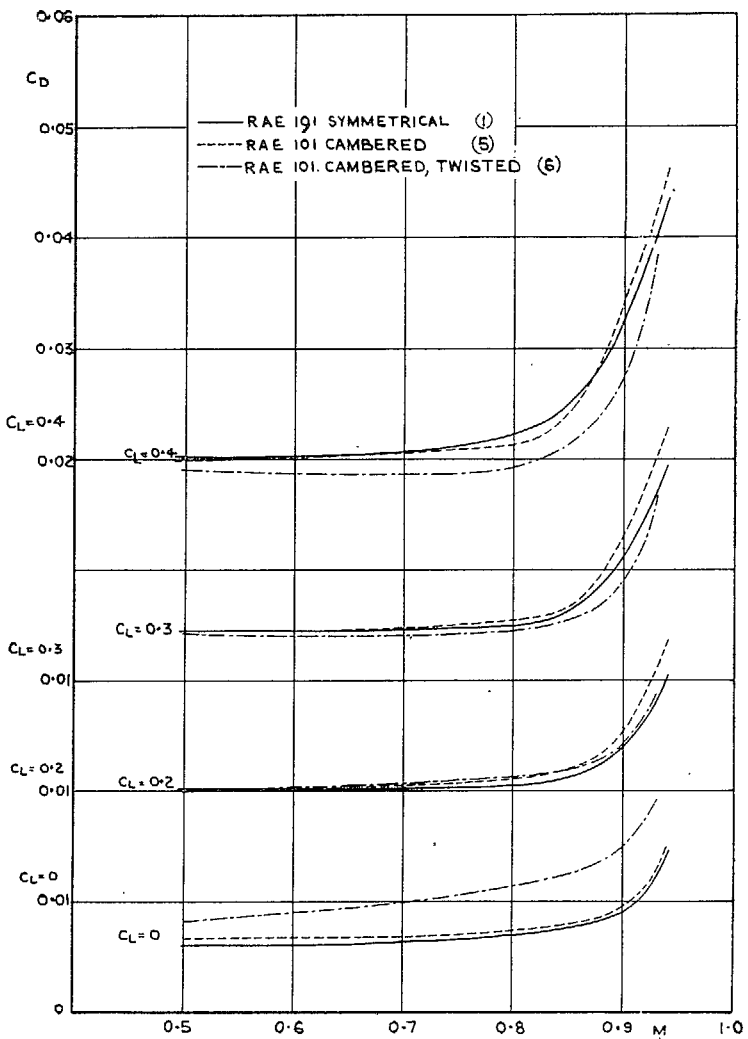

FIG. 6. C_D vs. M at constant C_L for the RAE 101 wings.

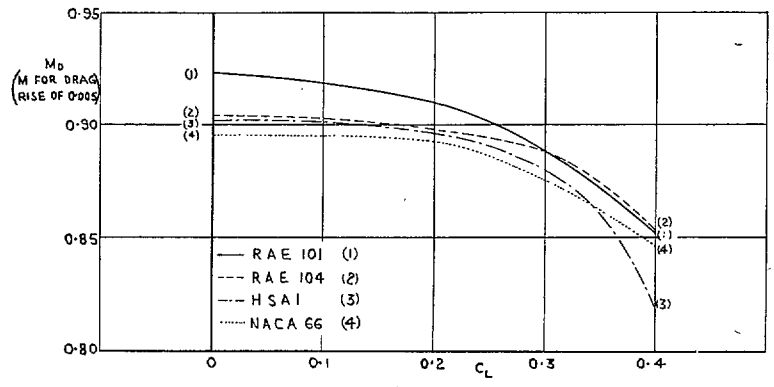

FIG. 7a. M_D vs. C_L for the symmetrical wings at $R = 2 \times 10^6$.

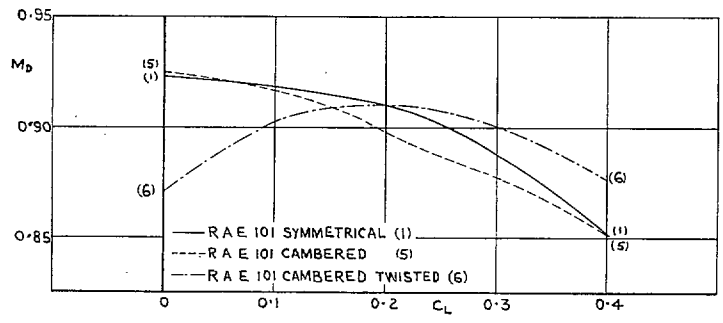

FIG. 7b. M_D vs. C_L for the RAE 101 section wings at $R = 2 \times 10^6$.

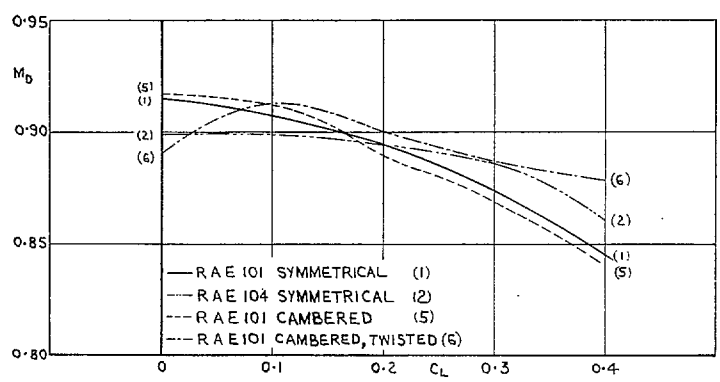

FIG. 7c. M_D vs. C_L for the wings tested at $R = 1 \times 10^6$.

FIGS. 7a, 7b and 7c. M_D vs. C_L curves.

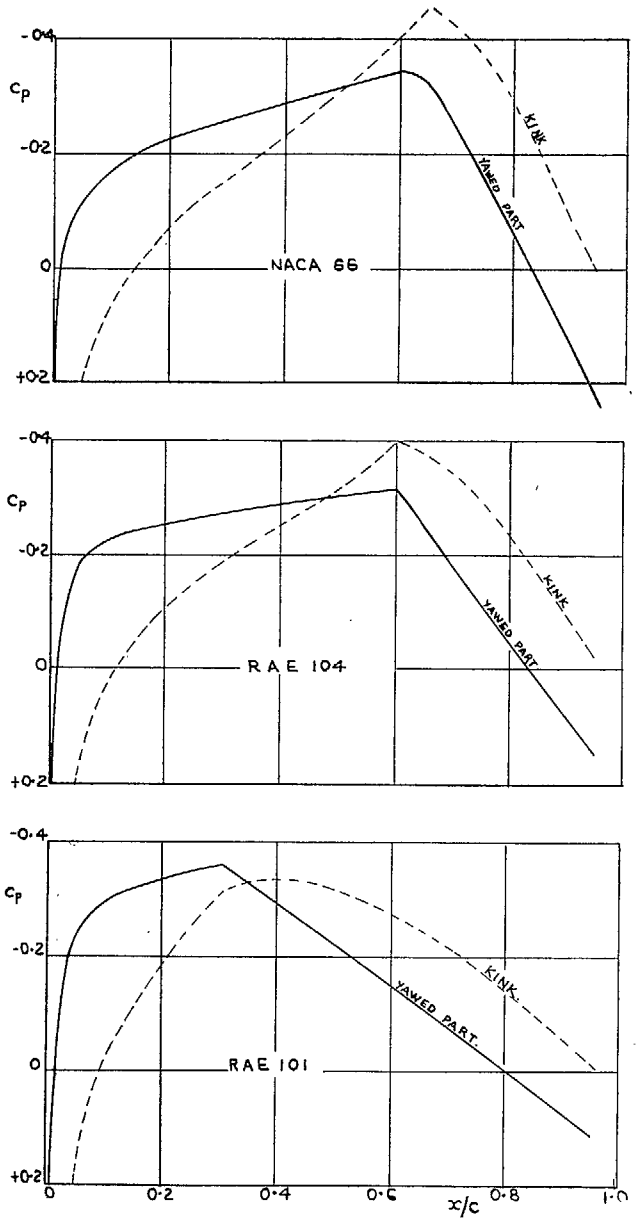

FIG. 8. Calculated pressure distributions at $C_L = 0$, $M = 0{\cdot}85$.

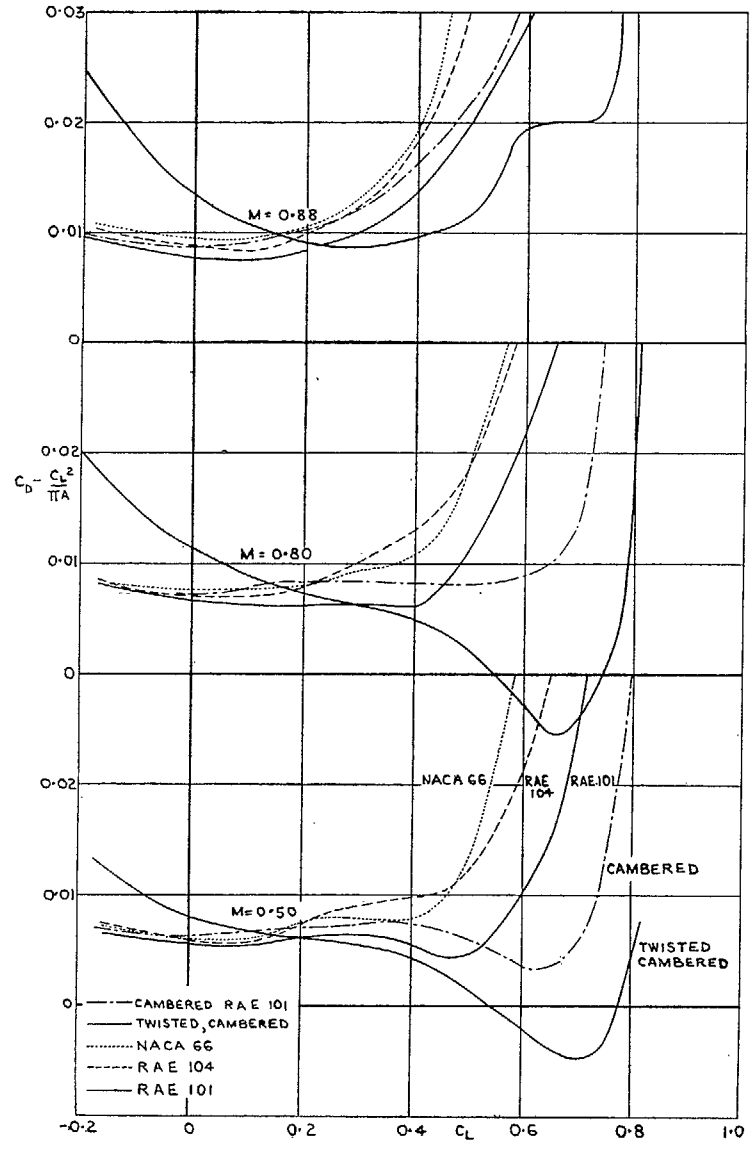

FIG. 9. $C_D - C_L^2/\pi A$ vs. C_L curves for several wings.

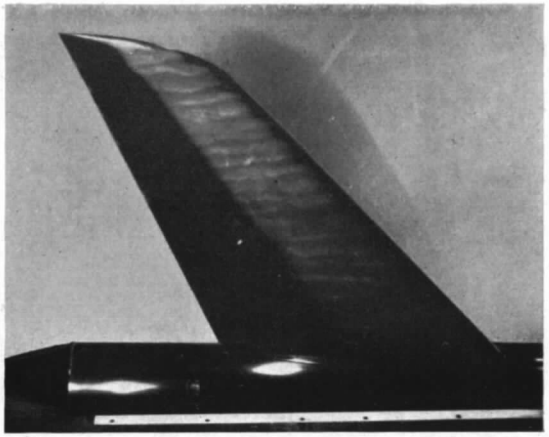

$M = 0{\cdot}5 \qquad C_L = 0$

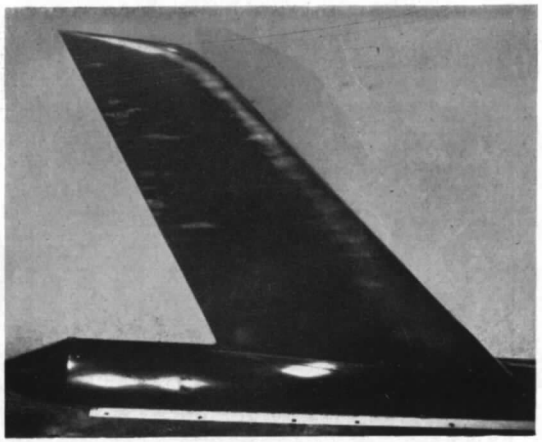

$M = 0{\cdot}5 \qquad C_L = 0{\cdot}25$

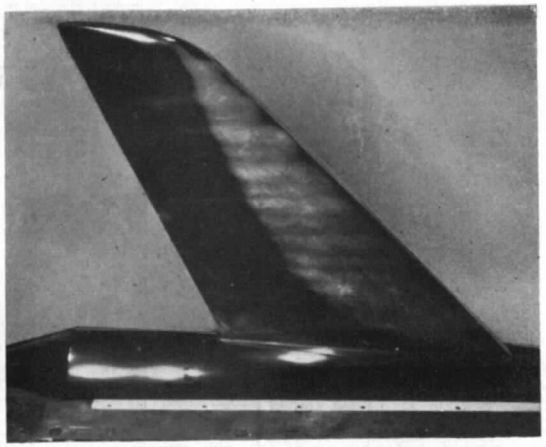

$M = 0{\cdot}88 \qquad C_L = 0{\cdot}29$

RAE 101

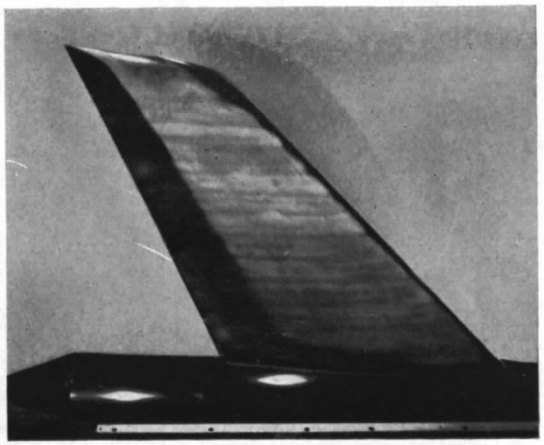

$M = 0{\cdot}5 \qquad C_L = 0$

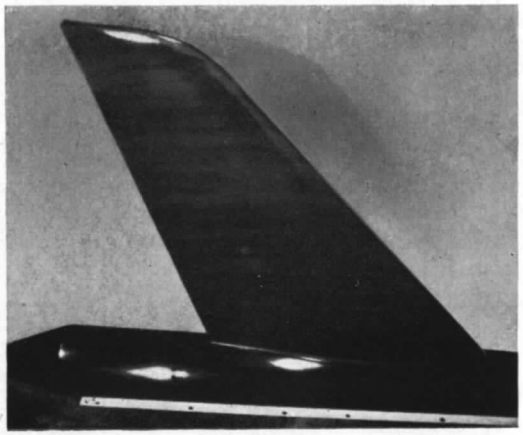

$M = 0{\cdot}5 \qquad C_L = 0{\cdot}24$

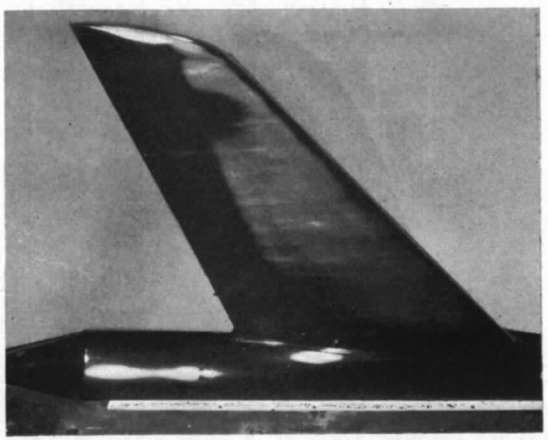

$M = 0{\cdot}88 \qquad C_L = 0{\cdot}25$

RAE 104

FIG. 10. Transition photographs for wings 1 and 2.

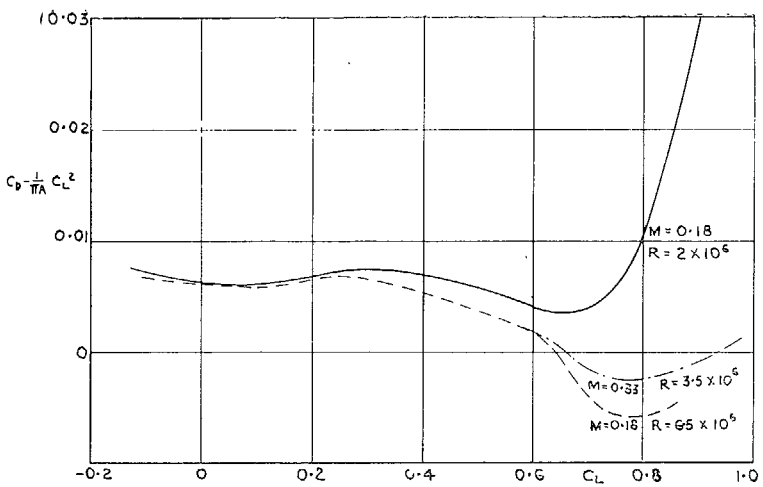

FIG. 11a. Reynolds number effects on $C_D - C_L^2/\pi A$.

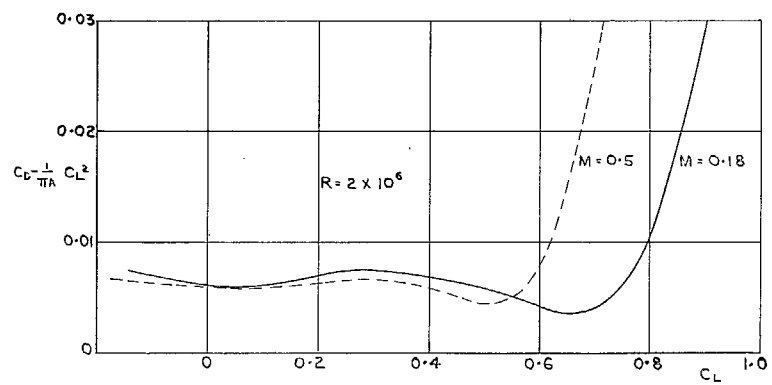

FIG. 11b. Mach number effects on $C_D - C_L^2/\pi A$ at $R = 2 \times 10^6$.

FIGS. 11a and 11b. $C_D - C_L^2/\pi A$ vs. C_L curves for wing No. 1 (RAE 101) at low speed.

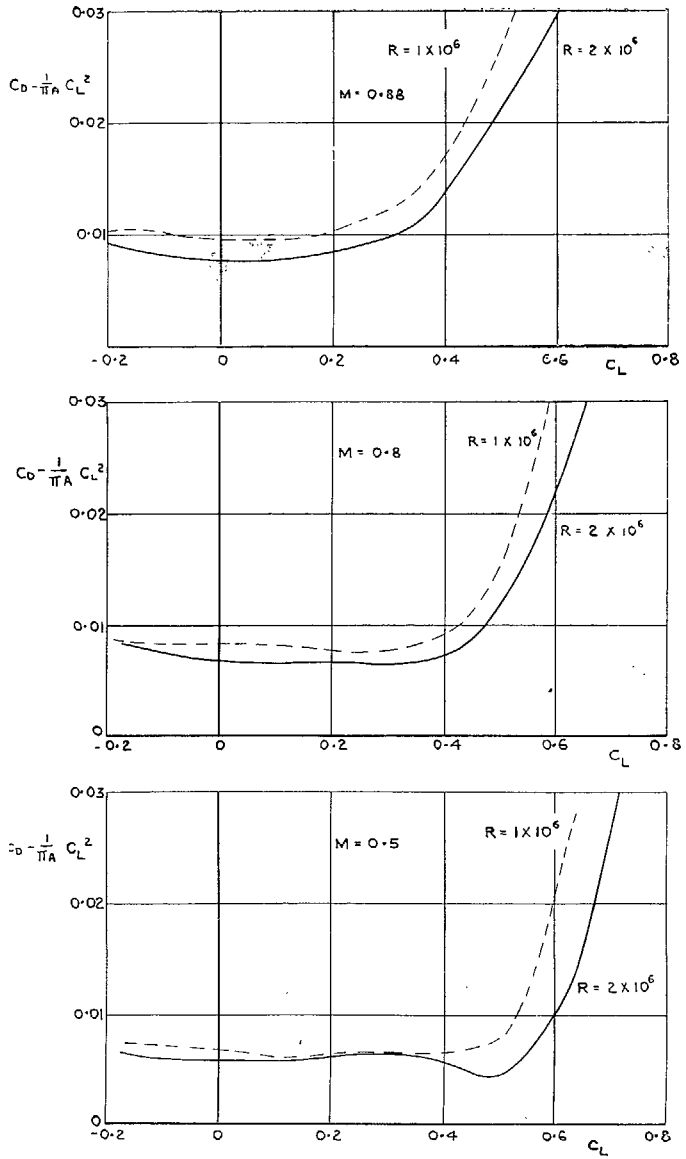

FIG. 12. $C_D - C_L^2/\pi A$ vs. C_L curves for wing No. 1 (RAE 101) showing Reynolds number effects at high speed.

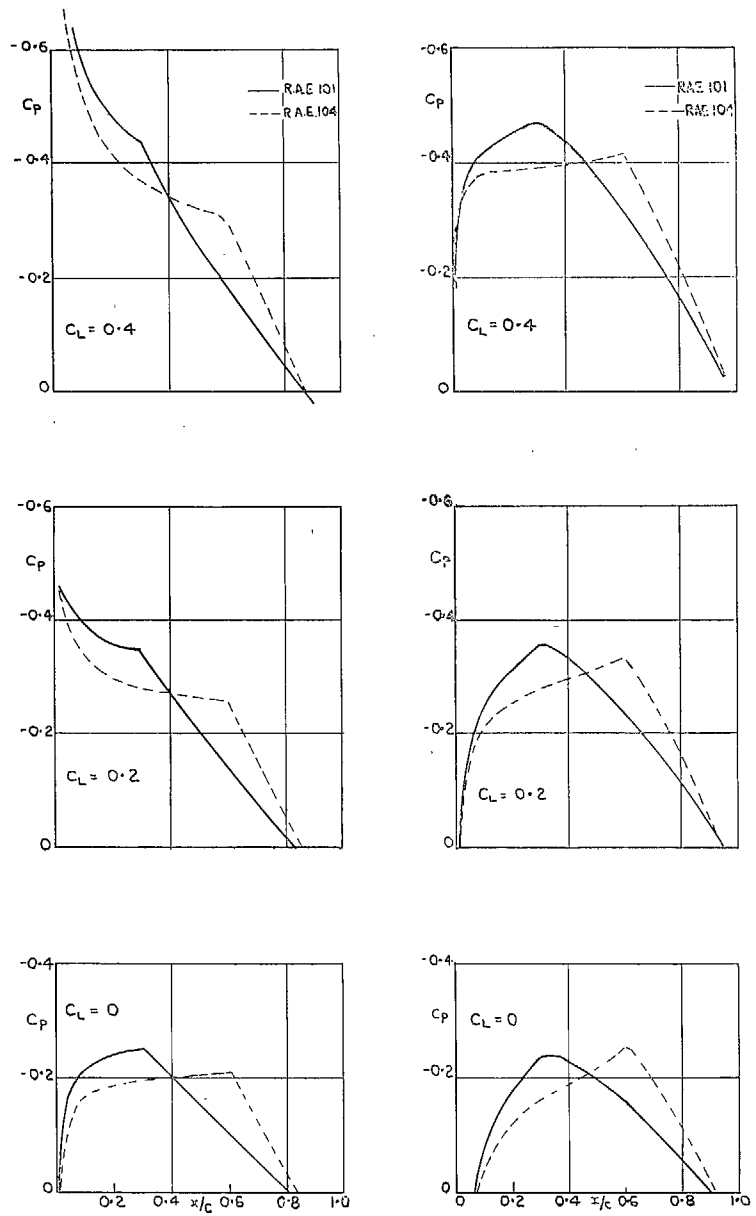

FIG. 13a. Yawed part of wing.

FIG. 13b. Kink section.

FIGS. 13a and 13b. Calculated pressure distributions at $M = 0$.

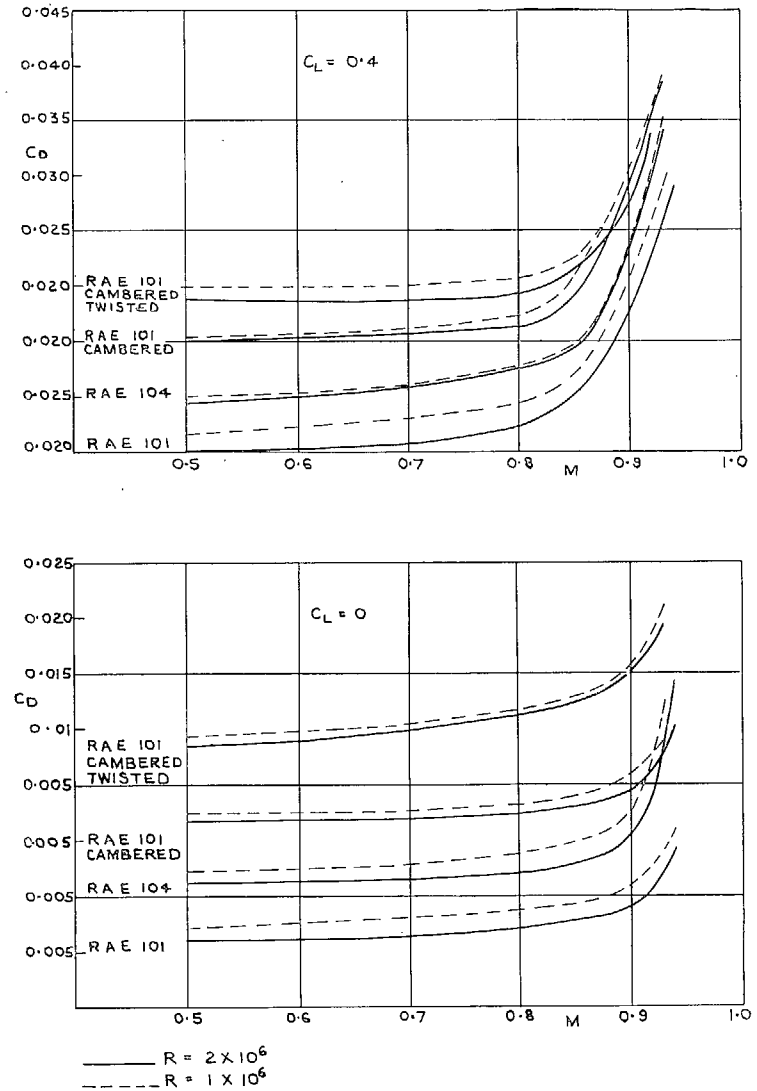

FIG. 14. C_D vs. M at $C_L = 0$ and 0·4, showing Reynolds number effects.

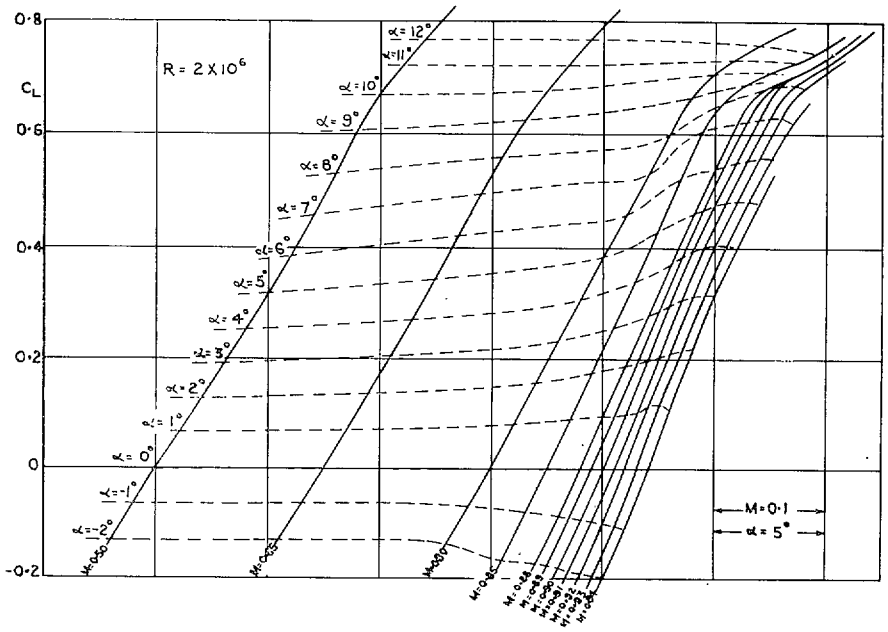

FIG. 15a. Lift carpet for wing No. 1 (RAE 101).

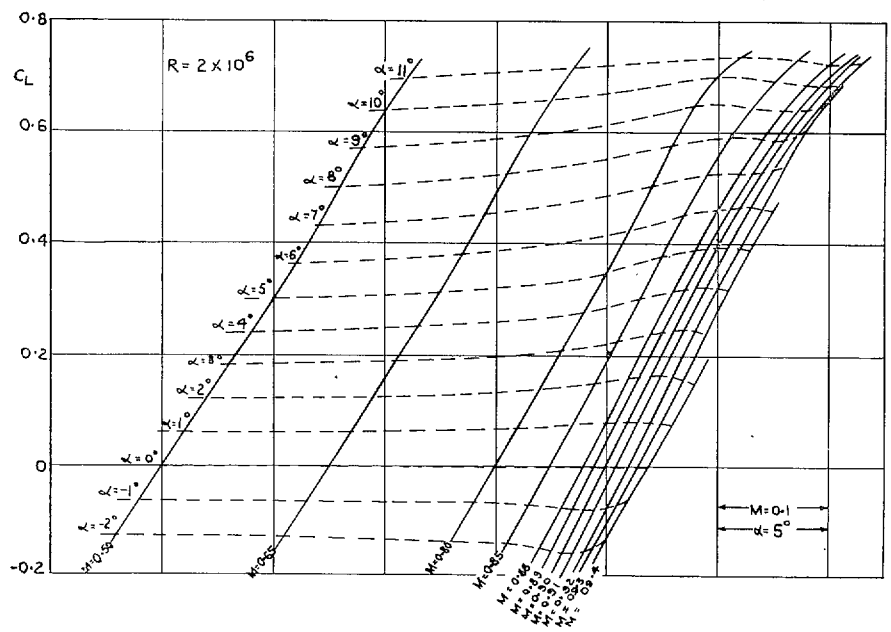

FIG. 15b. Lift carpet for wing No. 2 (RAE 104).

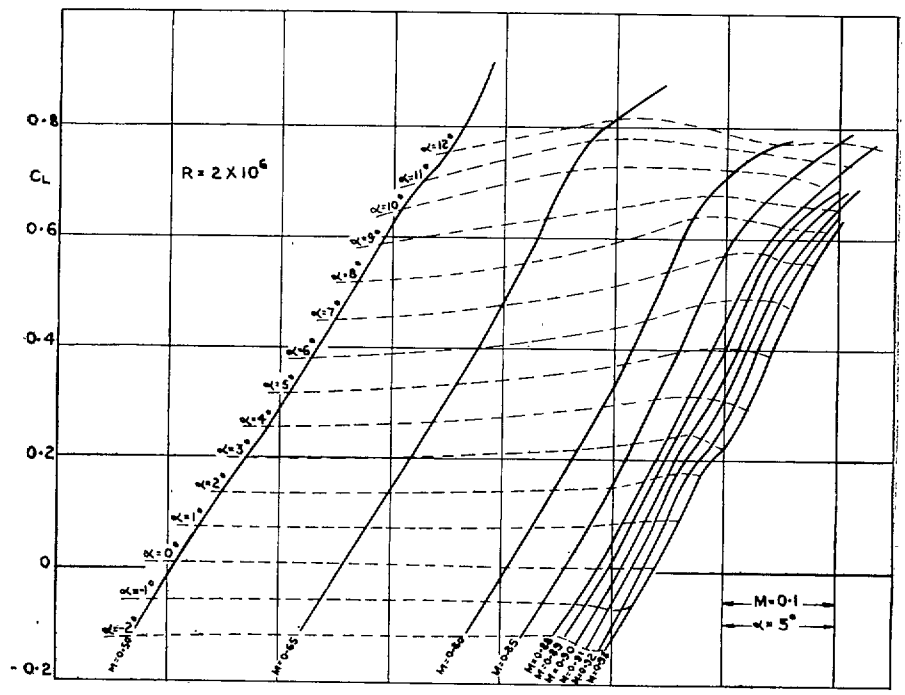

FIG. 16a. Lift carpet for wing No. 3 (HSA I).

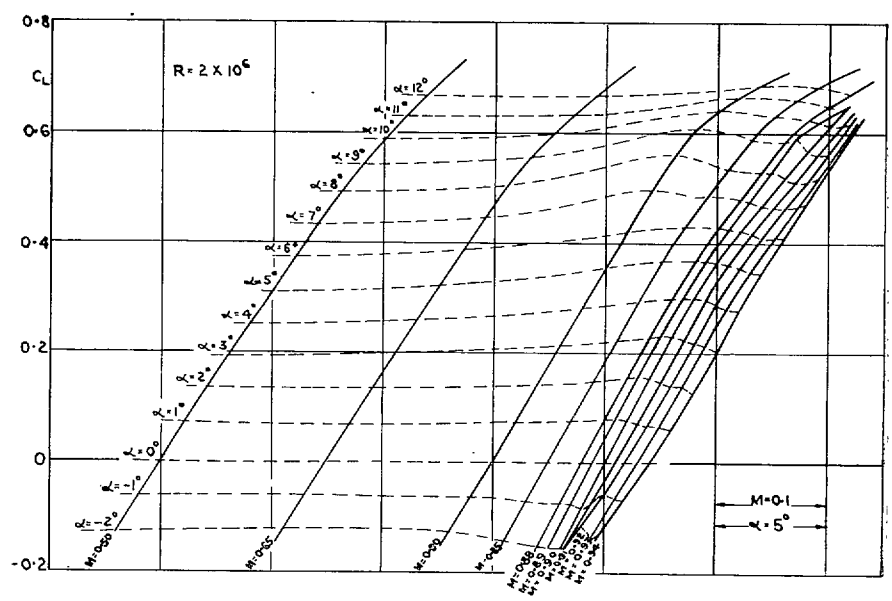

FIG. 16b. Lift carpet for wing No. 4 (NACA 66A-010).

C I

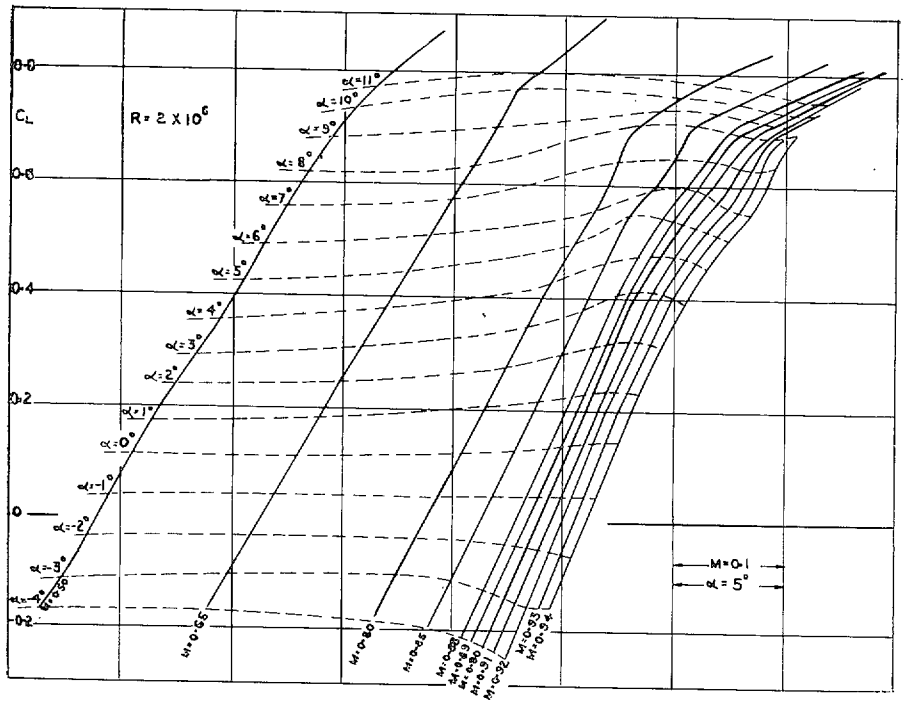

FIG. 17a. Lift carpet for wing No. 5 (cambered).

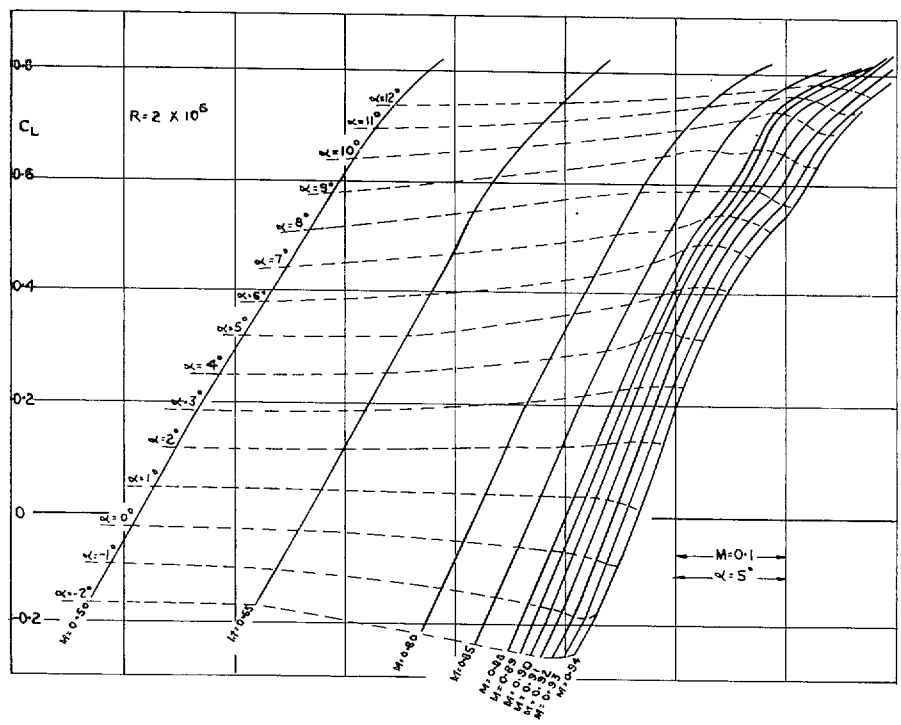

FIG. 17b. Lift carpet for wing No. 6 (twisted cambered).

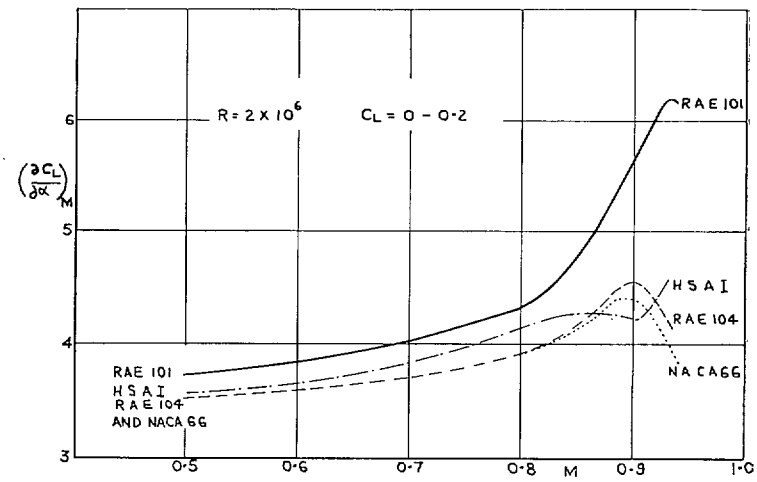

FIG. 18a. $(\partial C_L/\partial\alpha)_M$ vs. M for the symmetrical wings.

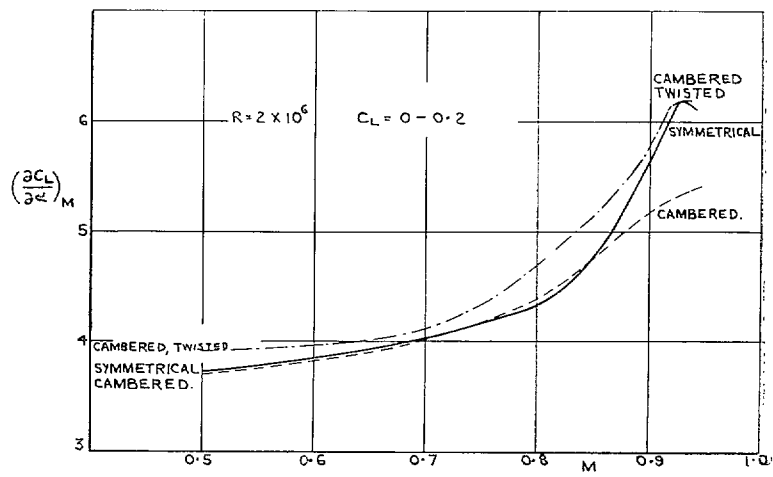

FIG. 18b. $(\partial C_L/\partial\alpha)_M$ vs. M for the RAE 101 wings.

FIGS. 18a and 18b. $(\partial C_L/\partial\alpha)_M$ vs. M curves for all the wings.

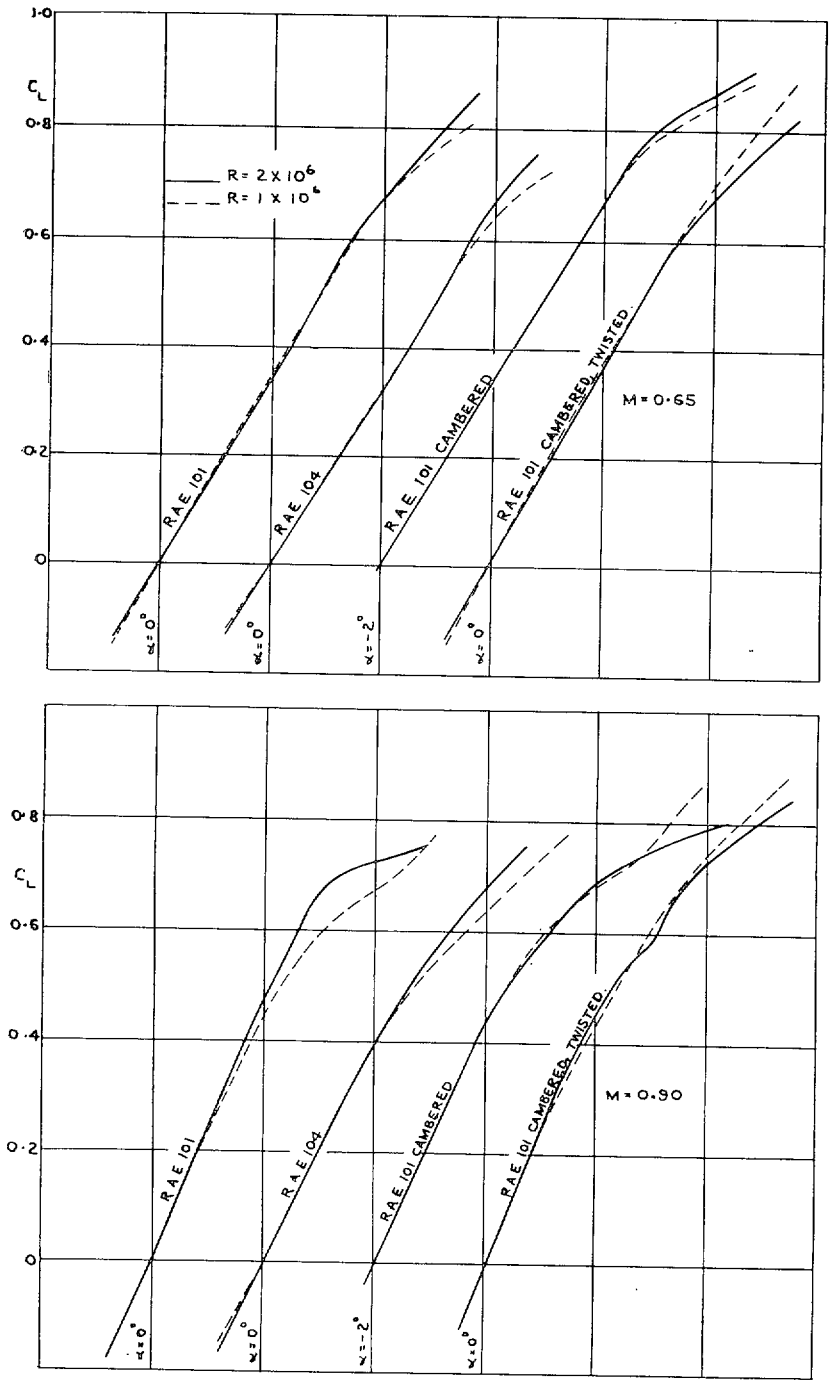

FIG. 19. C_L vs. α curves at constant Mach number, showing Reynolds number effects.

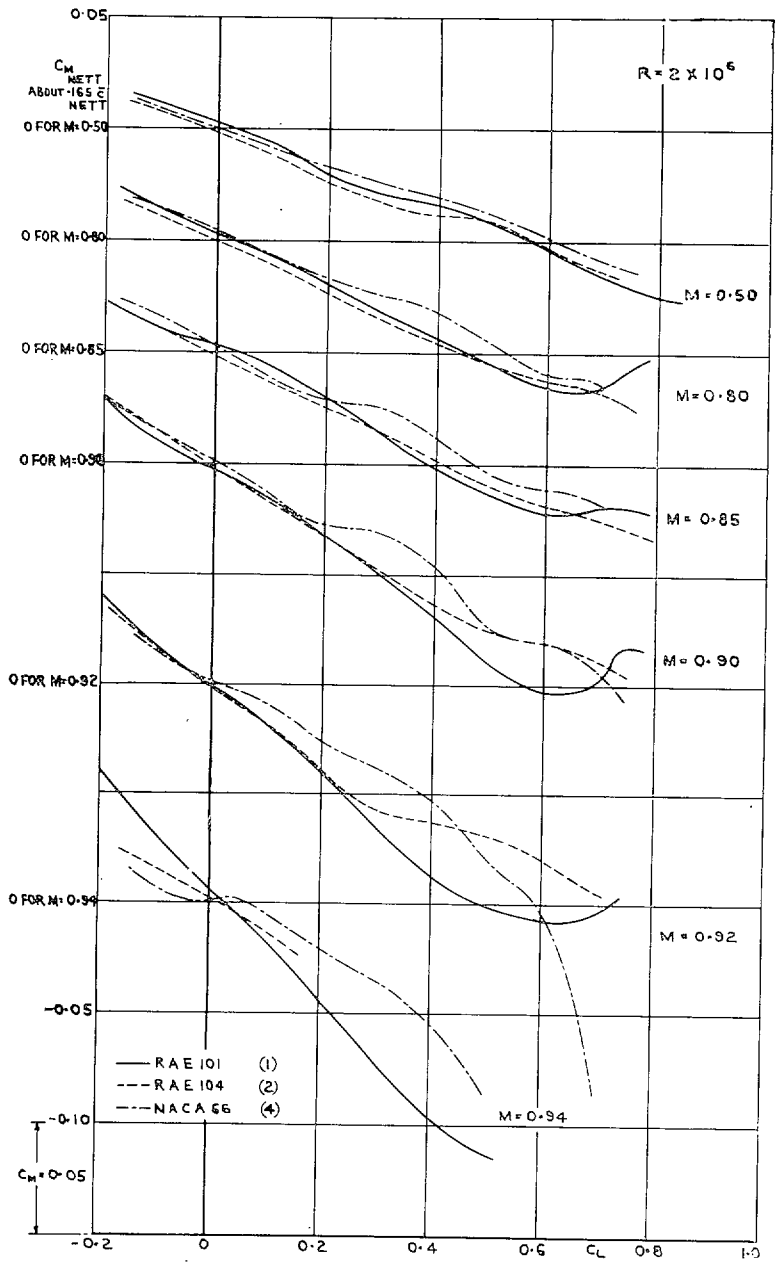

FIG. 20. C_m vs. C_L curves at constant Mach number for three symmetrical wings.

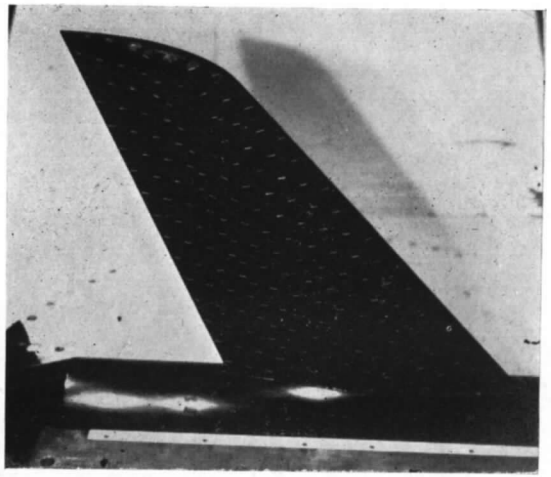

$M = 0{\cdot}88 \qquad C_L = 0{\cdot}34$

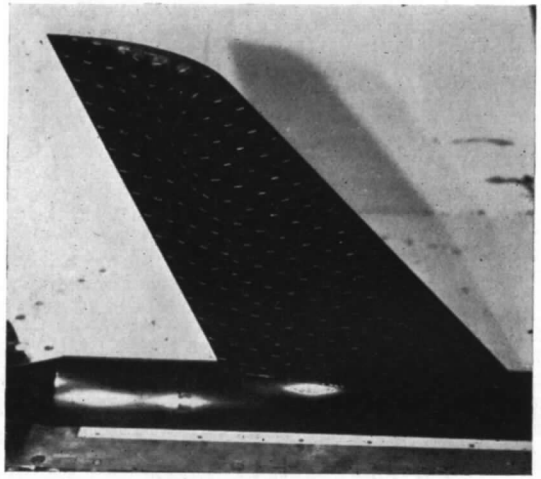

$M = 0{\cdot}90 \qquad C_L = 0{\cdot}36$

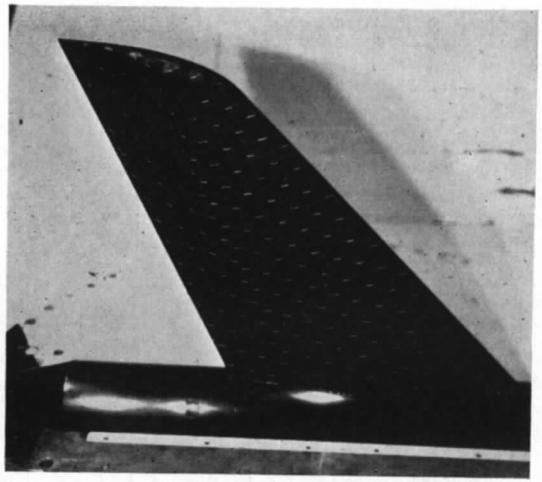

$M = 0{\cdot}92 \qquad C_L = 0{\cdot}37$

RAE 101

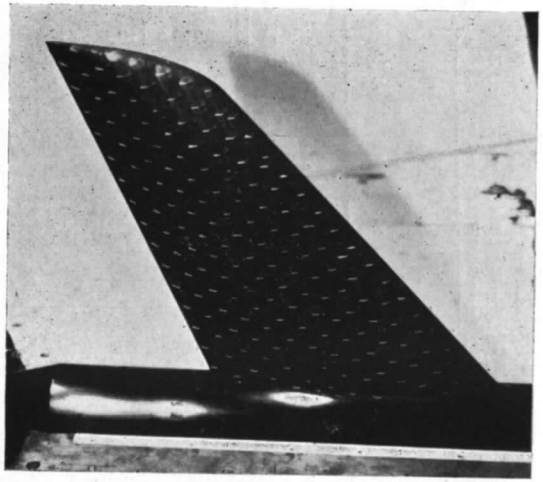

$M = 0{\cdot}88 \qquad C_L = 0{\cdot}29$

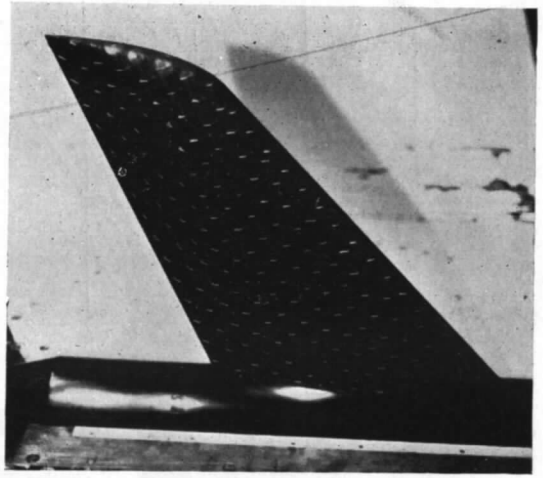

$M = 0{\cdot}90 \qquad C_L = 0{\cdot}30$

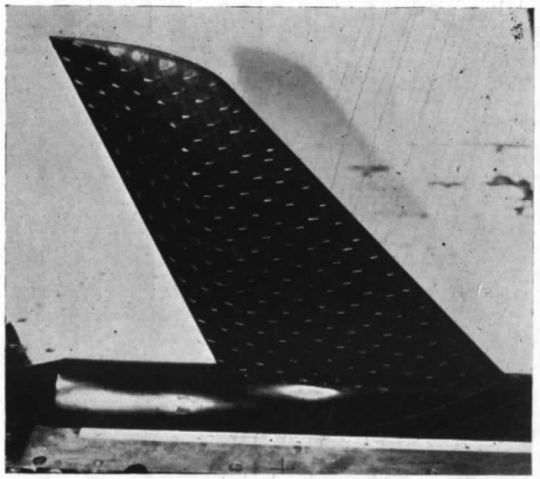

$M = 0{\cdot}92 \qquad C_L = 0{\cdot}30$

RAE 104.

FIG. 21. Surface tuft photographs for wings 1 and 2 at $\alpha = 3{\cdot}6$ deg.

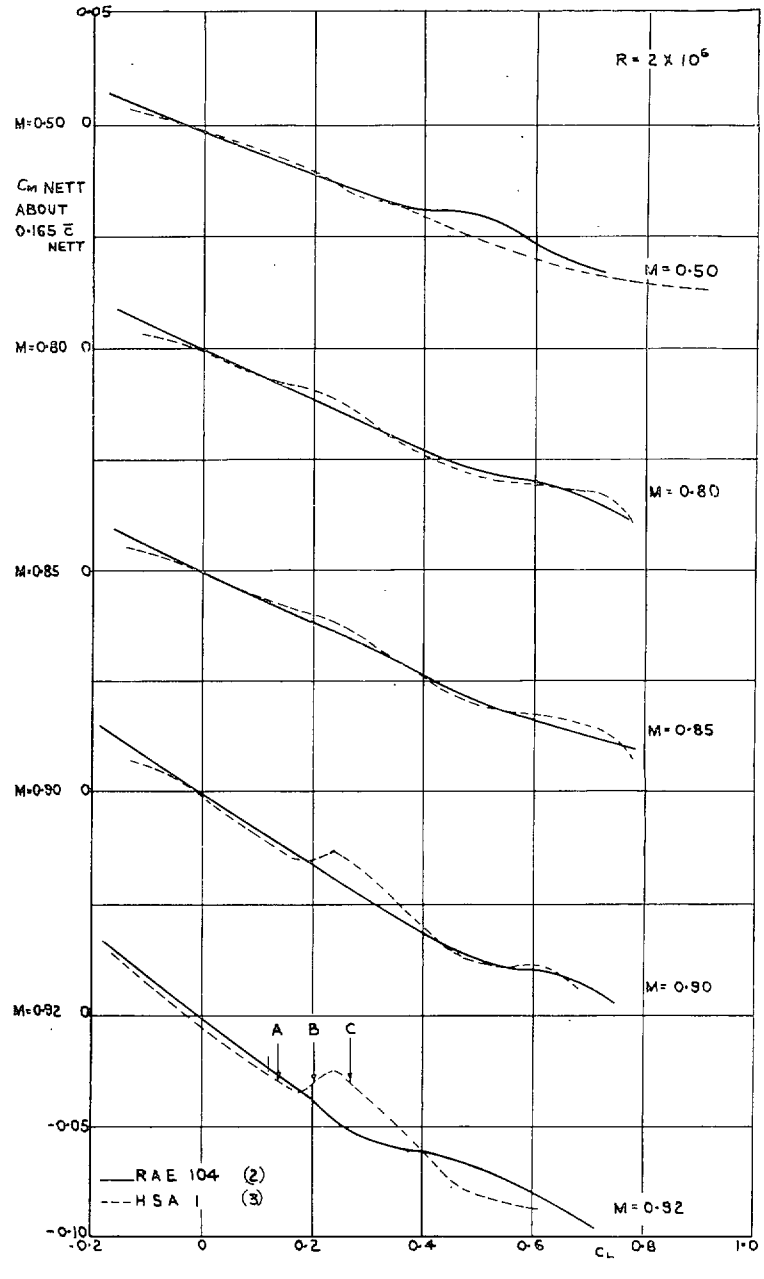

FIG. 22. C_m vs. C_L curves at constant Mach number for the RAE 104 and HSA I wings.

A. $C_L = 0{\cdot}14$

B. $C_L = 0{\cdot}20$

C. $C_L = 0{\cdot}27$

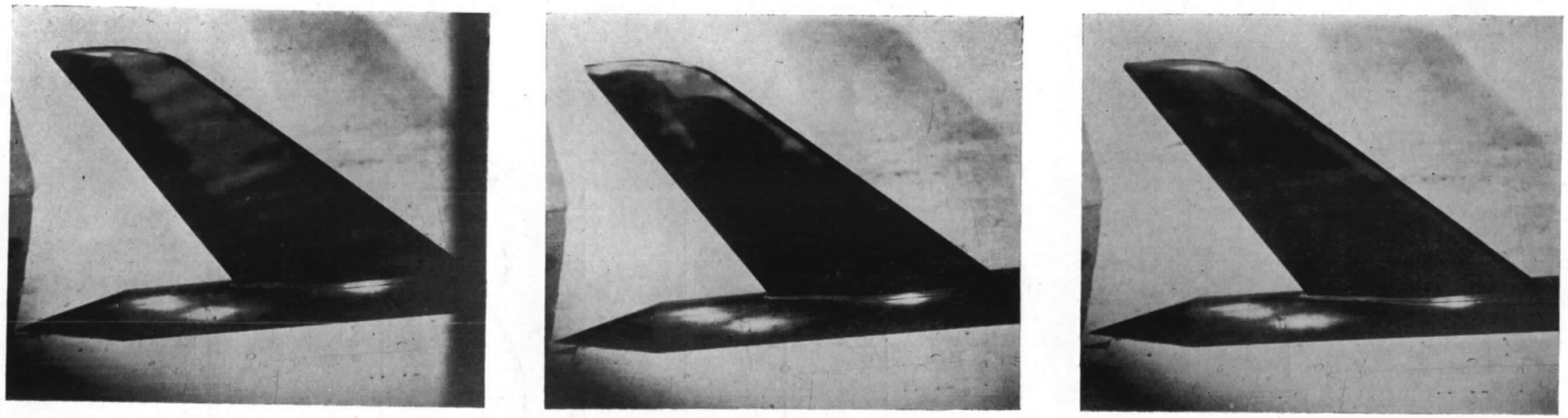

Upper surface.

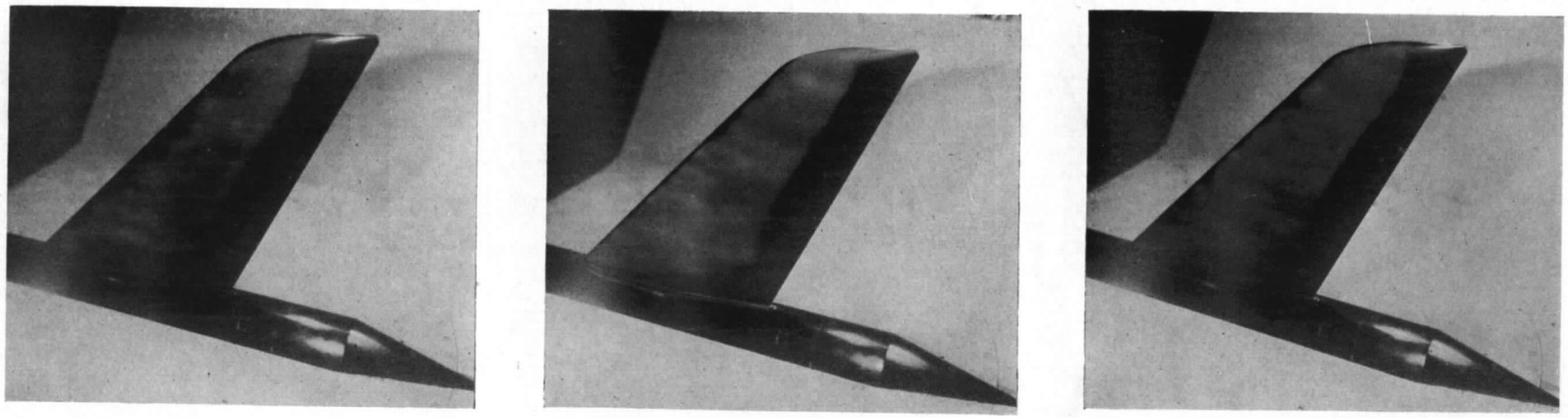

Lower surface.

FIG. 23. Transition photographs for wing No. 3 at $M = 0{\cdot}92$.

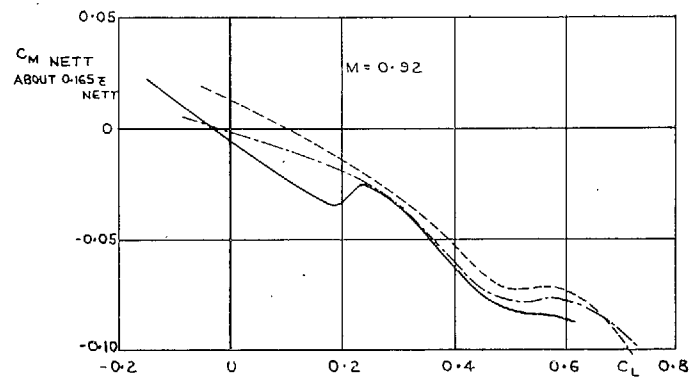

FIG. 24a. C_m vs. C_L curves.

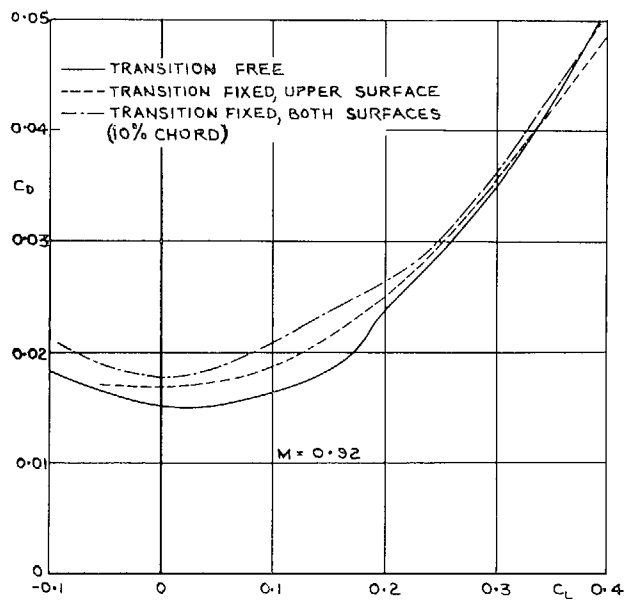

FIG. 24b. C_D vs. C_L curves.

FIGS. 24a and 24b. The effects on C_D and C_m of fixing transition on wing No. 3 (HSA I section).

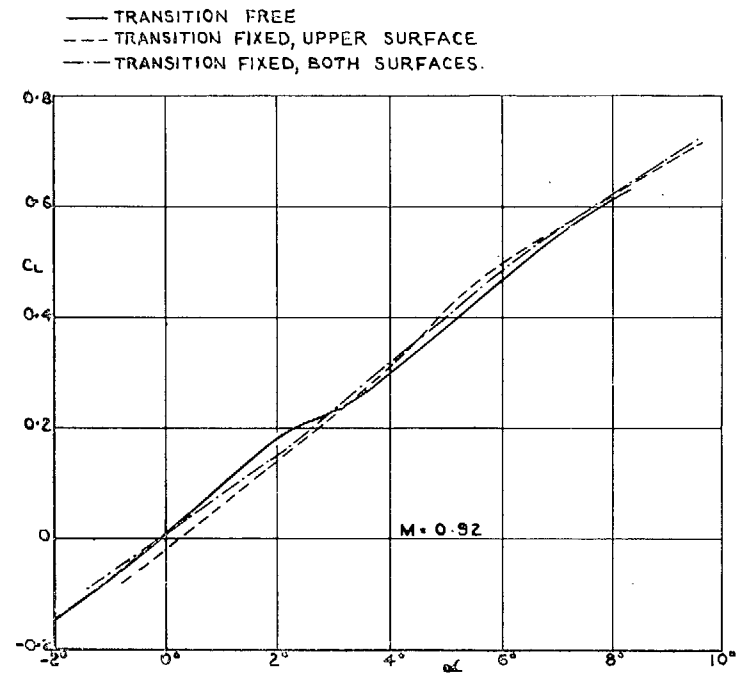

FIG. 25. The effect on C_L vs. α of fixing transition on wing No. 3 (HSA I section).

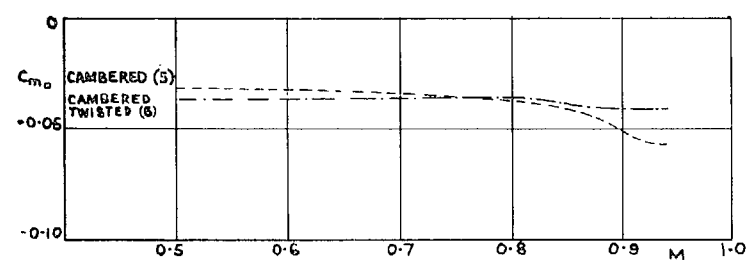

FIG. 26. The variation of C_{m_0} with M for wings Nos. 5 and 6.

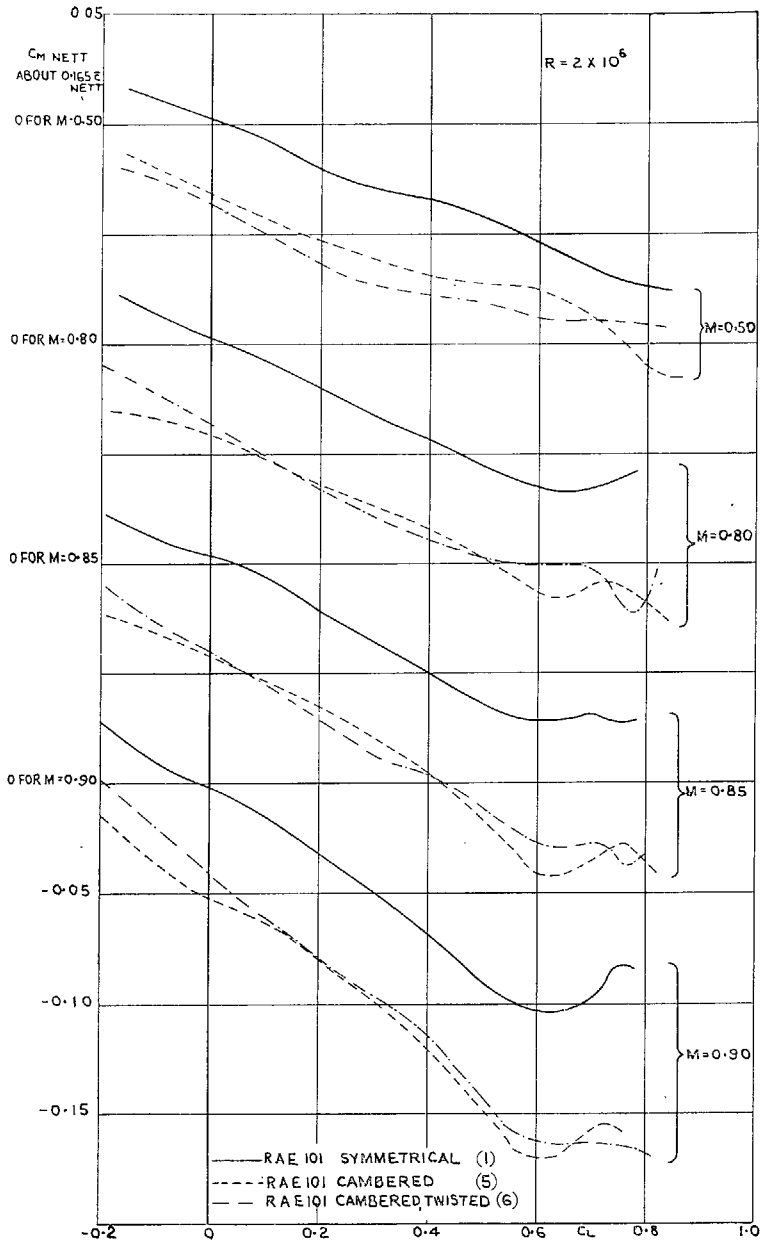

FIG. 27a. C_m vs. C_L curves at constant Mach number for the RAE 101 wings.

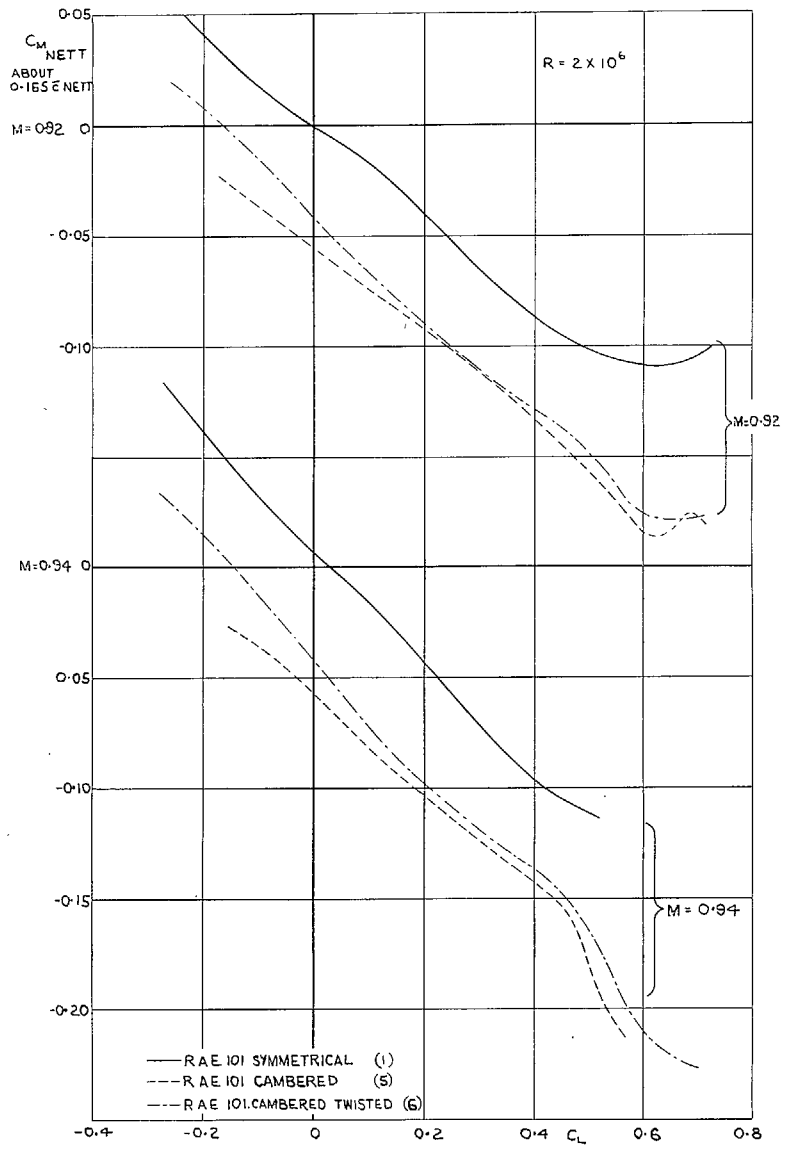

FIG. 27b. C_m vs. C_L curves at constant Mach number for the RAE 101 wings.

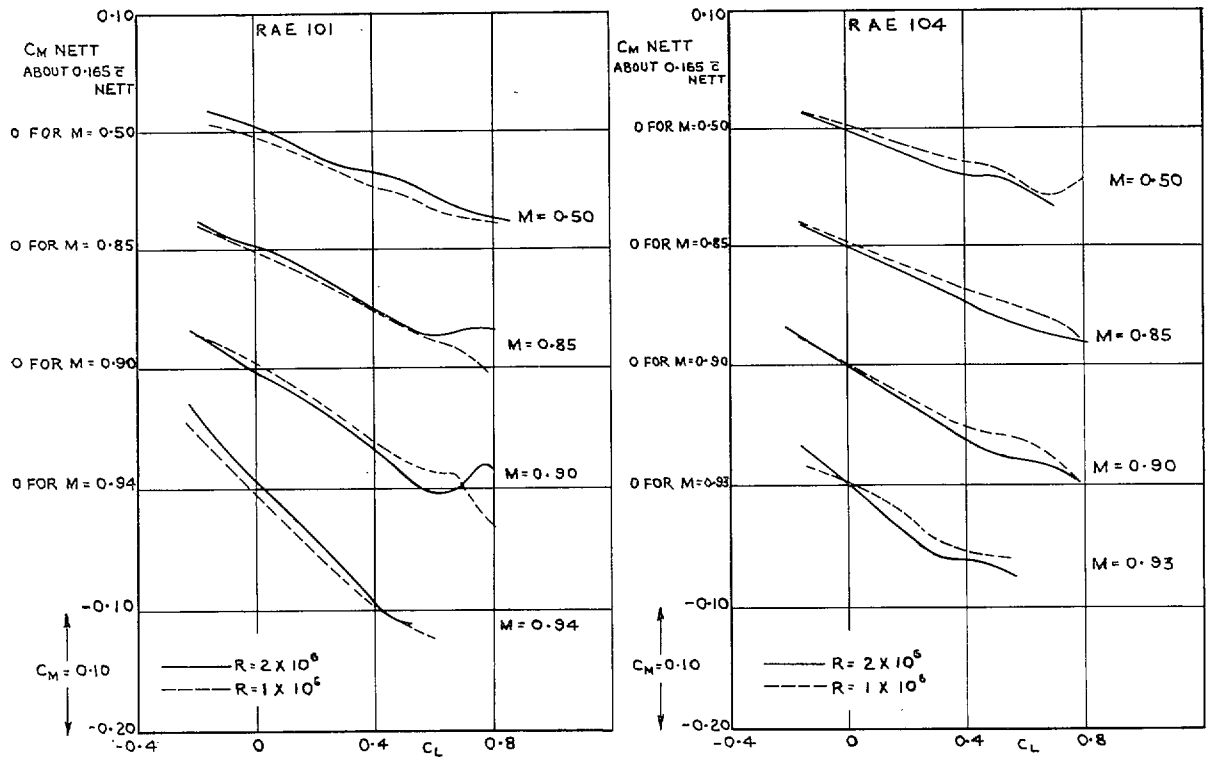

FIG. 28a. C_m vs. C_L curves at constant Mach number, showing Reynolds number effects.

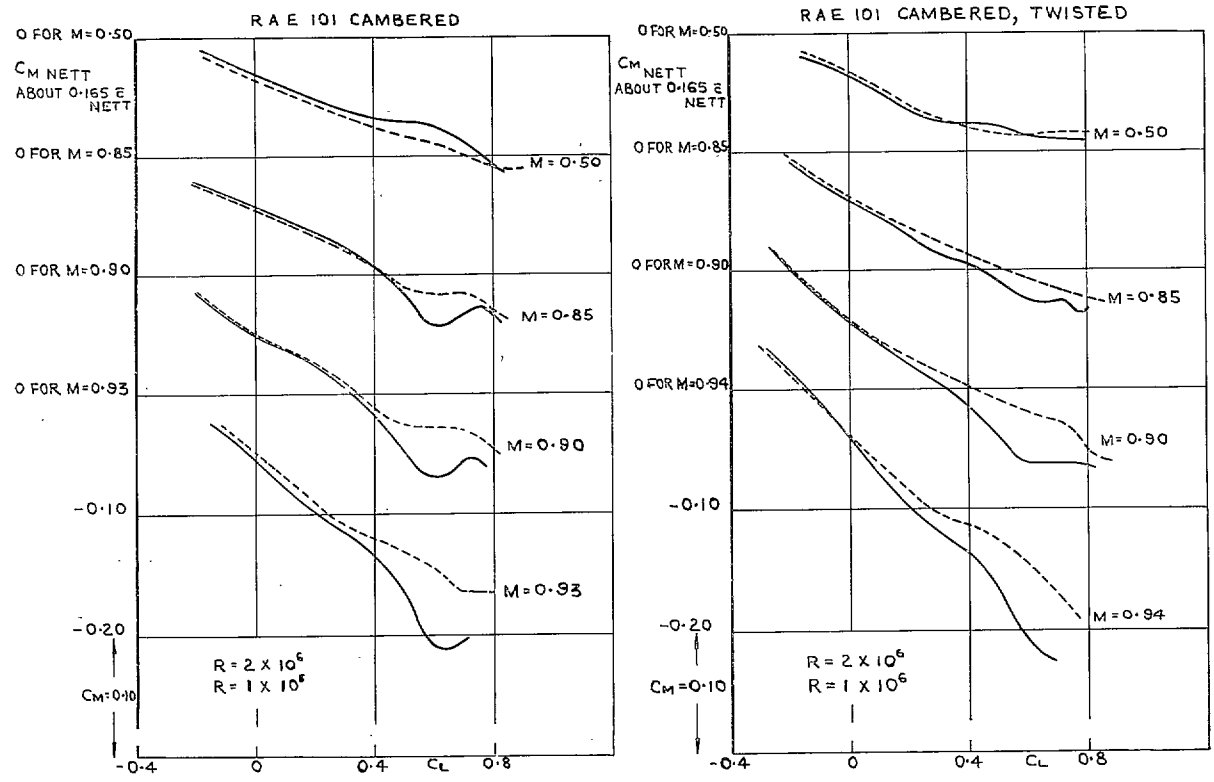

FIG. 28b. C_m vs. C_L curves at constant Mach number showing Reynolds number effects.

J4326 Wt.18/9296 K7 7/55 D&Co. 34/263

PRINTED IN GREAT BRITAIN

Publications of the Aeronautical Research Council

ANNUAL TECHNICAL REPORTS OF THE AERONAUTICAL RESEARCH COUNCIL (BOUND VOLUMES)

1936 Vol. I. Aerodynamics General, Performance, Airscrews, Flutter and Spinning. 40*s*. (41*s*. 1*d*).

Vol. II. Stability and Control, Structures, Seaplanes, Engines, etc. 50*s*. (51*s*. 1*d*.)

1937 Vol. I. Aerodynamics General, Performance, Airscrews, Flutter and Spinning. 40*s*. (41*s*. 1*d*.)

Vol. II. Stability and Control, Structures, Seaplanes, Engines, etc. 60*s*. (61*s*. 1*d*.)

1938 Vol. I. Aerodynamics General, Performance, Airscrews. 50*s*. (51*s*. 1*d*.)

Vol. II. Stability and Control, Flutter, Structures, Seaplanes, Wind Tunnels, Materials. 30*s*. (31*s*. 1*d*.)

1939 Vol. I. Aerodynamics General, Performance, Airscrews, Engines. 50*s*. (51*s*. 1*d*.)

Vol. II. Stability and Control, Flutter and Vibration, Instruments, Structures, Seaplanes, etc. 63*s*. (64*s*. 2*d*.)

1940 Aero and Hydrodynamics, Aerofoils, Airscrews, Engines, Flutter, Icing, Stability and Control, Structures, and a miscellaneous section. 50*s*. (51*s*. 1*d*.)

1941 Aero and Hydrodynamics, Aerofoils, Airscrews, Engines, Flutter, Stability and Control, Structures. 63*s*. (64*s*. 2*d*.)

1942 Vol. I. Aero and Hydrodynamics, Aerofoils, Airscrews, Engines. 75*s*. (76*s*. 3*d*.)

Vol. II. Noise, Parachutes, Stability and Control, Structures, Vibration, Wind Tunnels. 47*s*. 6*d*. (48*s*. 7*d*.)

1943 Vol. I. Aerodynamics, Aerofoils, Airscrews, 80*s*. (81*s*. 4*d*.)

Vol. II. Engines, Flutter, Materials, Parachutes, Performance, Stability and Control, Structures. 90*s*. (91*s*. 6*d*.)

1944 Vol. I. Aero and Hydrodynamics, Aerofoils, Aircraft, Airscrews, Controls. 84*s*. (85*s*. 8*d*.)

Vol. II. Flutter and Vibration, Materials, Miscellaneous, Navigation, Parachutes, Performance, Plates, and Panels, Stability, Structures, Test Equipment, Wind Tunnels. 84*s*. (85*s*. 8*d*.)

ANNUAL REPORTS OF THE AERONAUTICAL RESEARCH COUNCIL—

1933–34	1*s*. 6*d*. (1*s*. 8*d*.)	1937	2*s*. (2*s*. 2*d*.)
1934–35	1*s*. 6*d*. (1*s*. 8*d*.)	1938	1*s*. 6*d*. (1*s*. 8*d*.)
April 1, 1935 to Dec. 31, 1936.	4*s*. (4*s*. 4*d*.)	1939–48	3*s*. (3*s*. 2*d*.)

INDEX TO ALL REPORTS AND MEMORANDA PUBLISHED IN THE ANNUAL TECHNICAL REPORTS, AND SEPARATELY—

April, 1950 - - - - R. & M. No. 2600. 2*s*. 6*d*. (2*s*. 7½*d*.)

AUTHOR INDEX TO ALL REPORTS AND MEMORANDA OF THE AERONAUTICAL RESEARCH COUNCIL—

1909–1949 - - - - - R. & M. No. 2570. 15*s*. (15*s*. 3*d*.)

INDEXES TO THE TECHNICAL REPORTS OF THE AERONAUTICAL RESEARCH COUNCIL—

December 1, 1936 — June 30, 1939.	R. & M. No. 1850.	1*s*. 3*d*. (1*s*. 4½*d*.)
July 1, 1939 — June 30, 1945.	R. & M. No. 1950.	1*s*. (1*s*. 1½*d*.)
July 1, 1945 — June 30, 1946.	R. & M. No. 2050.	1*s*. (1*s*. 1½*d*.)
July 1, 1946 — December 31, 1946.	R. & M. No. 2150.	1*s*. 3*d*. (1*s*. 4½*d*.)
January 1, 1947 — June 30, 1947.	R. & M. No. 2250.	1*s*. 3*d*. (1*s*. 4½*d*.)
July, 1951 - - - -	R. & M. No. 2350.	1*s*. 9*d*. (1*s*. 10½*d*.)

Prices in brackets include postage.

Obtainable from

HER MAJESTY'S STATIONERY OFFICE

York House, Kingsway, London W.C.2 ; 423 Oxford Street, London W.1 (Post Orders : P.O. Box No. 569, London S.E.1) ; 13A Castle Street, Edinburgh 2 ; 39 King Street, Manchester 2 ; 2 Edmund Street, Birmingham 3 ; 109 St. Mary Street, Cardiff ; Tower Lane, Bristol 1 ; 80 Chichester Street, Belfast OR THROUGH ANY BOOKSELLER

S.O. Code No. 23-2930